DEVELOPMENT OF A PHYSICS-BASED MATHEMATICAL MODEL OF MICROPARTICLE SILICON BASED LITHIUM HALF CELLS

By

AL-MUSTASIN ABIR HOSSAIN

A thesis submitted in partial fulfillment of
the requirements for the degree of

MASTER OF SCIENCE IN MECHANICAL ENGINEERING

WASHINGTON STATE UNIVERSITY
School of Engineering and Computer Science, Vancouver

DECEMBER 2020

To the Faculty of Washington State University:

The members of the Committee appointed to examine the thesis of AL-MUSTASIN ABIR HOSSAIN find it satisfactory and recommend that it be accepted.

_____

Sun Ung Kim, Ph.D., Chair

_____

Linda (Xiaolin) Chen, Ph.D.

_____

Hua Tan, Ph.D.

ACKNOWLEDGMENT

I would like to thank my advisor Dr. Sun Ung Kim for his guidance and continuous support throughout this program, who provided significant aid throughout all experimental, numerical, and modeling aspects of these investigations. I would also like to thank my committee members, Dr. Linda (Xiaolin) Chen & Dr. Hua Tan.

I am grateful for the assistance provided by the mechanical engineering technicians Chad Swanson and Kurt Janzen, the lab technicians, each of whom helped ensure safe lab practices throughout my program.

Finally, I would like to thank my family members, my lab mates of Electrochemical Engineering Lab and friends of Washington State University who were always beside me and supported me throughout the journey.

DEVELOPMENT OF A PHYSICS-BASED MATHEMATICAL MODEL OF MICROPARTICLE SILICON BASED LITHIUM HALF CELLS

Abstract

by Al-Mustasin Abir Hossain, M.S.
Washington State University
December 2020

Chair: Sun Ung Kim

Lithium-ion batteries (LIBs) are considered as the most widely used energy storage systems. The energy density of the LIBs can be increased significantly if the graphite in anode can be replaced with silicon (Si) because Si's energy density, 3,579 [mAh/g], is much higher than graphite's, 372 [mAh/g]. However, during the lithiation-delithiation cycle, curves of electrode voltage *vs*. capacity differ and forms a hysteresis loop. This voltage hysteresis decreases power density of Si-based batteries. In 2013, Wang *et al*. reported that they made SiMP lithium half cells and ran lithiation-delithiation cycling experiments with different C-rates. They successfully demonstrated a self-healing chemistry of Si in battery applications. Their experiment also showed a voltage hysteresis during the cycling experiment of SiMP half cells. Similar to traditional LIBs, it was observed that the cell capacity decreases as the C-rate increases. In this work, a physics-based electrochemical model of the SiMP half-cell was developed to explain the causes of voltage gap in lithiation and delithiation cycles, and the capacity differences at different C-rates. To develop the model, at first, particular physics such as lithium diffusion, reaction kinetics, thermodynamics, and mechanical stress and strain was selected, and the relevant equations were

included in the model. To investigate the influence of hydrostatic stresses on electrochemical reactions in battery electrodes, a modified version of Butler-Volmer (BV) kinetics equation associated with hydrostatic stress was implemented in the model. Besides, Verburgge & Cheng's analytical approach was applied to identify the importance of mechanical stress in the voltage hysteresis of Si-anode batteries in lithiation-delithiation cycles. Then, literature surveys were conducted to get the physical properties required to make the model a physics-based one. The previously reported parameters such as solid diffusivity, exchange current density, Young's modulus, Poisson's ratio, and partial molar volume were found. Finally, the electrochemical model investigated the impact of hydrostatic stress on the output voltage of the SiMP half cells. In addition, the model was used to identify performance limitations. By checking the impact of the key parameters on the voltage curves during battery cycling, the model provided the possible reasons of voltage differences during lithiation and delithiation.

TABLE OF CONTENTS

LIST OF TABLES

LIST OF FIGURES

CHAPTER 1: INTRODUCTION

1.1 Overview of Lithium-Ion-Batteries with Silicon Anodes (LIBs)

Lithium-ion batteries (LIBs) are highly regarded as one of the most broadly used secondary battery systems. In comparison to other rechargeable batteries, such as nickel-cadmium and nickel-metal hydride batteries, LIBs are featured with higher energy density, higher operating voltages, limited self-discharging and lower maintenance requirements [1]. However, the current traditional graphite anode cannot meet the demand on energy density, operation reliability and system amalgamation arising from portable electronic devices, electric vehicles, and energy storage applications. Graphite anodes demonstrate only a moderate intrinsic specific capacity (372 [mAh/g]) and serious safety issues due to lithium plating and further formation of lithium dendrites [2]. Subsequently, studies on new generation anode materials with the characteristics of high capacities, a proper charging/discharging potential, as well as safe and low-cost manufacturing and usage have attracted great attention [3]. Among all potential lithium-ion battery (LIB) anodes, silicon (Si) is one of the most prominent candidates to replace graphite due to the following reasons: (1) Si has the highest gravimetric capacity (3600 [mAh/g], lithiated to $Li_{4.4}Si$) [4] and volumetric capacity (9786 [mAh/cm^3], calculated based on the initial volume of Si) other than lithium metal; (2) Si displays an appropriate discharge voltage at ca. 0.4 [V] in average, which finds a good quality balance between retaining reasonable open-circuit voltage (OCV) and evading adverse lithium plating process [5]; (3) Si is abundant (second richest in earth crust), potentially low cost, environment friendly, and non-toxic [6]. However, drastic volume expansion (around 300% for $Li_{4.4}Si$) [7] and huge stress generation are accompanied with the lithiation/delithiation process of Si, which causes series of severe destructive consequences [5]. (i) Electrode structure

integrity is deteriorated due to gradually enhanced pulverization during repeated lithiation/delithiation processes; (ii) disconnection between an electrode and current collector is induced by the interfacial stress; (iii) continuous consumption of lithium ions occurs during the continuous formation-breaking-reformation process of solid electrolyte interface (SEI) layer [8]. All these processes accelerate electrode collapse and capacity fading in a harmonious way. Besides, the critical problem of volume expansion, the poor intrinsic electron conductivity of Si also contributes to the sluggish electrochemical kinetics [9].

Table-1.1: Different potential anode materials for Lithium-Ion batteries (LIBs) [1-9]

Anode Material	Specific Capacity [mAh/g]	Volume Change (%)	Benefits	Challenges
Silicon	3,600	320	Highest energy density	Capacity fade due to damage from expansion and contraction
Aluminum	2,235	604	Better energy density than graphite	Worse energy density and more expansion than silicon
Tin	990	252	Stabler than silicon	Worse energy density than silicon
Graphite	372	10	Stable; widely used	Poor energy density

To tackle the aforementioned critical issues, tremendous efforts have been made since 1990s [10]. The strategies developed include utilizing nanoscale silicon, compositing with stress-relief buffer matrix, and constructing a physical compartment to accommodate volume expansion.

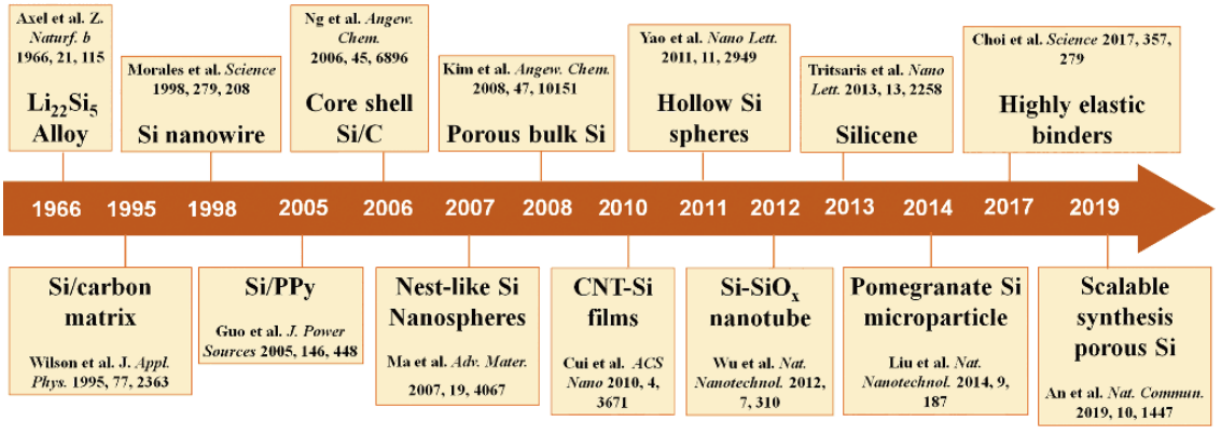

Figure-1.1: Timeline of selected important breakthroughs in silicon-based anode[10].

In recent years, numerous battery models have been developed which can calculate hydrostatic stress generation in lithium-insertion materials due to lithium insertion and extraction.[11] The maximum stress in a lithium insertion particle has a tendency to be nearly proportional to the concentration gradient developed in the particle, multiplied by the particle size. To be precise, the difference in concentrations between the surface and center of the particle determines, the maximum stress to a great degree. Christensen and Newman [12] demonstrated that the hydrostatic stress increases with the dimensionless current, which is proportional to the particle size and C-Rate and inversely proportional to the solid phase diffusivity.

The set of equations that is used to compute hydrostatic stress includes a coupling between diffusion and elasticity along with the appropriate material and momentum balances. Garcia et al. [13] developed a two-dimensional (2D) porous electrode model that also reported for potential and

ion concentration distributions in the electrolyte. However, their work used transport equations derived from dilute solution theory, which is generally not suitable for Li-ion systems, and their diffusion equation did not include the pressure driving force that gives rise to chemo-mechanical or electro-chemo-mechanical coupling.

Zhang et al. [14] developed a semi-analytic expression for the hydrostatic stress distribution in a spherical particle as a function of solid-phase lithium concentration, which allowed a decoupling of the diffusion and elasticity equations. They extended their one-dimensional (1D) model to a finite-element COMSOL multi-physics model that could compute hydrostatic stress in ellipsoids of arbitrary aspect ratio. However, their Fick's (2^{nd} law) mass diffusion equation was strictly valid only for dilute solutions, neglected the influence of a moving boundary, and they did not include the correct form of the pressure driving force for diffusion. In the following paper, Zhang et al. [11] explored both intercalation stress and heat generation in single particles.

Christensen and Newman [12] developed a set of one dimensional (1D) equations for a spherical particle, which included moving boundary considerations and was based on the more rigorous multicomponent diffusion equation developed by Hirschfelder et al. and Curtiss [15] and Bird. This diffusion equation is valid for concentrated solutions, such as the solid solutions formed in Li-intercalation materials, and properly handles the contribution of pressure gradients to the driving force for diffusion. In Addition to that, a more general, nonlinear version of Hooke's law was utilized. Though computationally more expensive than other approaches, this model has the advantage of applicability to insertion materials that undergo massive volumetric changes (e.g., Li_xSi or Li_xSn alloys), in which second-order terms in Hooke's law and convection terms and

pressure driving forces in the diffusion equation become important. In another paper, hydrostatic stress generation at two-phase boundaries was also explored.[16] In 2008, Verbrugge and Cheng [17] presented a modification to the approach of Sastry et al. [18] that included surface energy considerations. The surface energy manifests itself as a boundary condition of finite compressive stress at the surface of a particle, which becomes important for nanomaterials (<~50 nm diameter). Christensen and Newman [12] exhibited that a compressive external stress could reduce the likelihood of particle fracture, because the fracture threshold for the tensile stress is typically much lower than for the compressive stress.

In our work, we developed a physics-based mathematical model to identify voltage hysteresis during battery lithiation-delithiation cycling of lithium-ion based silicon anode half-cells. We wanted to make our model as simple as possible. Therefore, we started with a one-dimensional single spherical particle model. First, we used mass diffusion equation (Fick's 2nd Law). Then added boundary conditions. Next, we modified the Butler-Volmer (BV) equation likewise Jin et al. [19] adding hydrostatic stress-induced voltage. Cheng and Verbrugge [17] developed an analytical solution for hydrostatic stress calculation. Stress induced voltage was generated form this stress. Since we have noticed ~300% volume expansion during battery cycling in silicon anode-based cells, radius of the spherical particle will also be expanded. Therefore, we introduced state of charge (SOC) based particle radius equation in our model. How it works, is discussed later in this thesis. Including Jin et al. [19], many other groups have developed mathematical models for Si anode, but to the best of knowledge, no one has included SOC dependent radius equation in their model, we are the first one to do so. Li et al. [20] discussed diffusivities cannot be same throughout the battery cycling.

Therefore, we added asymmetric diffusivity and exchange current density like two different values in each cycle. One value was used for lithiation and another different value for delithiation which nobody has done that before. We also validated our model with experimental results. The purpose of our work here is to identify voltage hysteresis during battery cycling of silicon anode cell and identify the main reason behind voltage hysteresis using our physics-based mathematical model.

1.2 References

[1] J. Tarascon, M. Armand, Issues and challenges facing rechargeable lithium batteries, Nature. 414 (2001) 359-367. doi:10.1038/35104644.

[2] W. Zhang, A review of the electrochemical performance of alloy anodes for lithium-ion batteries, Journal of Power Sources. 196 (2011) 13-24. doi:10.1016/j.jpowsour.2010.07.020.

[3] K. Abraham, Prospects and Limits of Energy Storage in Batteries, The Journal of Physical Chemistry Letters. 6 (2015) 830-844. doi:10.1021/jz5026273.

[4] B. Boukamp, G. Lesh, R. Huggins, All-Solid Lithium Electrodes with Mixed-Conductor Matrix, Journal of The Electrochemical Society. 128 (1981) 725-729. doi:10.1149/1.2127495.

[5] B. Liang, Y. Liu, Y. Xu, Silicon-based materials as high capacity anodes for next generation lithium ion batteries, Journal of Power Sources. 267 (2014) 469-490. doi:10.1016/j.jpowsour.2014.05.096.

[6] H. Wu, Y. Cui, Designing nanostructured Si anodes for high energy lithium ion batteries, Nano Today. 7 (2012) 414-429. doi:10.1016/j.nantod.2012.08.004.

[7] L. Beaulieu, K. Eberman, R. Turner, L. Krause, J. Dahn, Colossal Reversible Volume Changes in Lithium Alloys, Electrochemical And Solid-State Letters. 4 (2001) A137. doi:10.1149/1.1388178.

[8] S. Ng, J. Wang, D. Wexler, K. Konstantinov, Z. Guo, H. Liu, Highly Reversible Lithium Storage in Spheroidal Carbon-Coated Silicon Nanocomposites as Anodes for Lithium-Ion Batteries, Angewandte Chemie International Edition. 45 (2006) 6896-6899. doi:10.1002/anie.200601676.

[9] M. Ashuri, Q. He, L. Shaw, Silicon as a potential anode material for Li-ion batteries: where size, geometry and structure matter, Nanoscale. 8 (2016) 74-103. doi:10.1039/c5nr05116a.

[10] H. Ma, F. Cheng, J. Chen, J. Zhao, C. Li, Z. Tao et al., Nest-like Silicon Nanospheres for High-Capacity Lithium Storage, Advanced Materials. 19 (2007) 4067-4070. doi:10.1002/adma.200700621.

[11] X. Zhang, A. Sastry, W. Shyy, Intercalation-Induced Stress and Heat Generation within Single Lithium-Ion Battery Cathode Particles, Journal of The Electrochemical Society. 155 (2008) A542. doi:10.1149/1.2926617.

[12] J. Christensen, J. Newman, Stress generation and fracture in lithium insertion materials, Journal of Solid State Electrochemistry. 10 (2006) 293-319.

[13] R. García, Y. Chiang, W. Craig Carter, P. Limthongkul, C. Bishop, Microstructural Modeling and Design of Rechargeable Lithium-Ion Batteries, Journal of The Electrochemical Society. 152 (2005) A255.

[14] X. Zhang, W. Shyy, A. Marie Sastry, Erratum: Numerical Simulation of Intercalation-Induced Stress in Li-Ion Battery Electrode Particles [J. Electrochem. Soc., 154, A910 (2007)], Journal of The Electrochemical Society. 154 (2007) S21.

[15] J. Hirschfelder, C. Curtiss, R. Bird, Molecular Theory of Gases and Liquids, Physics Today. 8 (1955) 17-17. doi:10.1063/1.3061949.

[16] J. Christensen, J. Newman, A Mathematical Model of Stress Generation and Fracture in Lithium Manganese Oxide, Journal of The Electrochemical Society. 153 (2006) A1019. doi:10.1149/1.2185287.

[17] M. Verbrugge, Y. Cheng, Stress Distribution within Spherical Particles Undergoing Electrochemical Insertion and Extraction, ECS Transactions. 16 (2019) 127-139. doi:10.1149/1.2987765.

[18] X. Zhang, W. Shyy, A. Marie Sastry, Numerical Simulation of Intercalation-Induced Stress in Li-Ion Battery Electrode Particles, Journal of The Electrochemical Society. 154 (2007) A910. doi:10.1149/1.2759840.

[19] C. Jin, H. Li, Y. Song, B. Lu, A. Soh, J. Zhang, On stress-induced voltage hysteresis in lithium ion batteries: Impacts of surface effects and inter-particle compression, Science China Technological Sciences. 62 (2019) 1357-1364. doi:10.1007/s11431-018-9491-6.

[20] J. Li, N. Dudney, X. Xiao, Y. Cheng, C. Liang, M. Verbrugge, Asymmetric Rate Behavior of Si Anodes for Lithium-Ion Batteries: Ultrafast Delithiation versus Sluggish Lithiation at High Current Densities, Advanced Energy Materials. 5 (2014) 1401627. doi:10.1002/aenm.201401627.

[21] A.A. Hossain, Y. Cha, M. Song, S.U. Kim, Side Reaction Correction and Non-linear Exchange Current Density for Mathematical Modeling of Silicon Anode Based Lithium-Ion Batteries, (2020). doi:10.13140/RG.2.2.36674.40646.

CHAPTER 2: RESEARCH MOTIVATION

2.1 Large Volume Expansion Phenomenon

The lifespan and performance of lithium-ion batteries are related to the mechanical expansion and contraction of the active materials, particularly for silicon-enhanced negative electrodes. Baker et al. [1] developed a model to describe how lithium diffuses within lithiated silicon, and they included the influence of active material expansion (upon lithiation) and contraction (upon delithiation). The treatment of diffusion is based on irreversible thermodynamics, and a charge-transfer relationship is used at the electrode−electrolyte interface. In their experiment, CR2032 coin cells were assembled with the Si thin film as the working electrode and a lithium foil as the counter-reference electrode. For the potential sweeps, the product vT_{point} (ν being the scan rate and T_{point} being the time per point) was kept constant and equal to 1 [mV]/point. The experimental method allowed to isolate their analysis to the active material and avoided the necessity of treating binders, conductive diluents, and complicated geometries associated with conventional porous electrodes used in most practical lithium-ion batteries and in the construction and modelling of a Li−Si porous electrode. The model is shown to compare favourably with experimental results. Details have been discussed at chapter 2.

Based on the studies of Wu and Cui [2] and others [3-6] three fundamental materials challenges are outlined to using Si as a viable battery electrode, as illustrated in Figure-2.1. Material pulverization is a common scenario in Si anodes. The large volume expansion/contraction during lithium insertion/extraction induces large stresses. These stresses can cause cracking and pulverization of the Si, which leads to loss of electrical contact and eventual capacity fading

(Figure-2.1a). Morphology and volume change of the whole Si electrode is another important issue. The large volume changes also cause significant challenges at the level of the entire electrode. During lithiation, Si particles expand and impinge on each other. During delithiation, Si particles contract, which can result in detachment of their surrounding electrical connections. This drastic electrode morphology change can further contribute to capacity fading. In addition, the total volume of the whole Si anode also increases and decreases upon lithiation and delithiation, leading to electrode peel-off and failure, which creates challenges for full cell design.

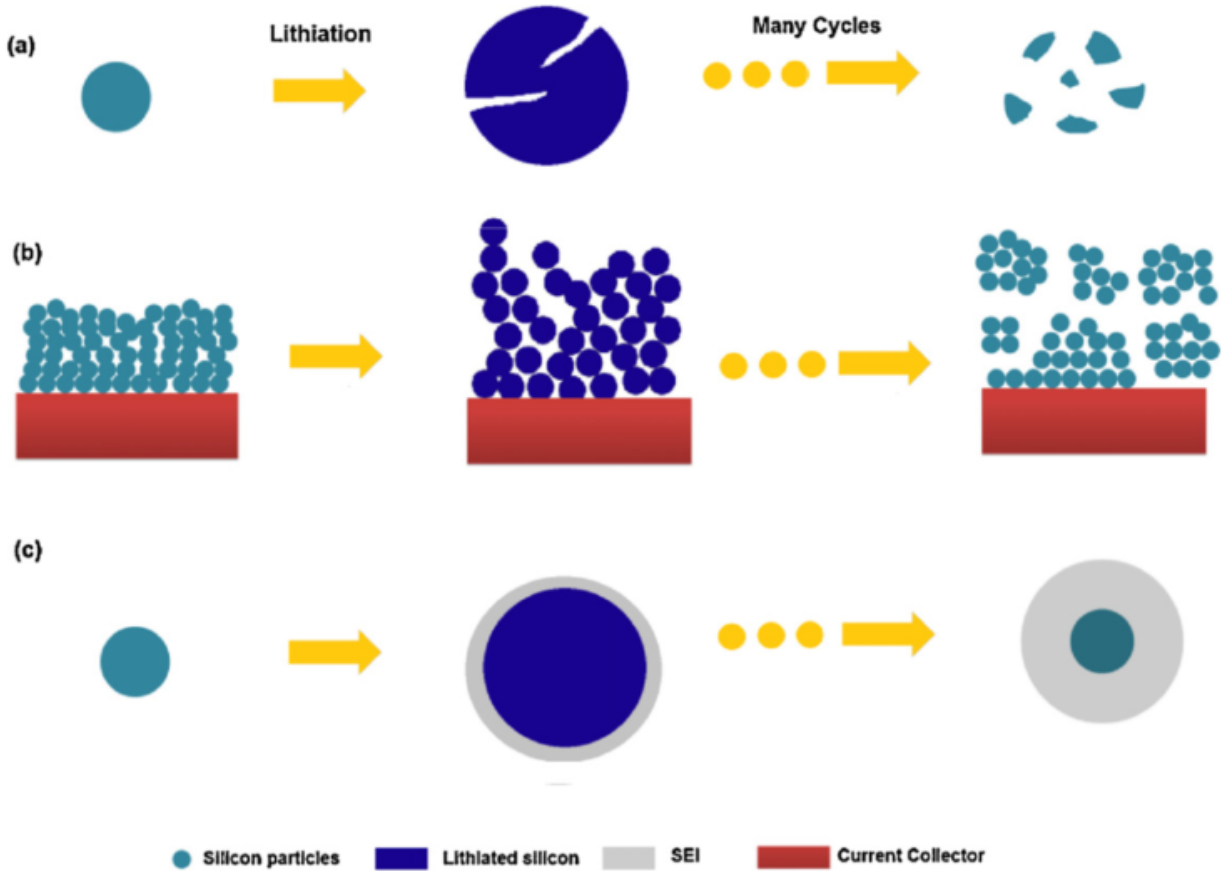

Figure-2.1: Si Electrode failure mechanisms: Material Pulverization (a); Morphology & volume change of the entire Si Electrode (b); Continues SEI growth (c) [2]

Solid-electrolyte interphase (SEI) development around the spherical particle is also detrimental to Si anode-based LIBs. When the potential of the anode is below ~1 [V] versus Li/Li^+, the decomposition of the organic electrolyte at the electrode surface is thermodynamically favourable. The decomposition product forms a layer on the electrode material surface called the ‘‘solid-electrolyte interphase’’ (SEI). The SEI stability at the interface between Si and the liquid electrolyte is a critical factor for obtaining long cycle life. However, the large volume change makes it very challenging to form a stable SEI. As illustrated in Figure-2.1b, Si particles expand out towards the electrolyte upon lithiation and contract during delithiation. The SEI formed in the lithiated (expanded) state can be broken as the particle shrinks during delithiation. This re-exposes the fresh Si surface to the electrolyte and the SEI forms again, resulting in thicker and thicker SEI upon charge/discharge cycling (Figure-2.1c).

2.2 Voltage Hysteresis Identification

One of the key challenges associated with Silicon anode-based Lithium-Ion Batteries (LIBs) is the emergence of voltage difference between lithiation and delithiation. During battery cycling experiment of silicon anode Cell, a huge voltage gap is seen. This phenomenon is known as “voltage hysteresis”. Various researchers have conducted several experiments with voltage hysteresis. Bertotti et al. [7] narrated at their work, “Whatever the physical system considered, hysteresis phenomena are always the sure indication that the system is living for long times in states that are far from thermodynamic equilibrium. Therefore, in principle, the observed behavior should be interpreted in the frame of nonequilibrium thermodynamics. This goal has not yet been achieved because of the many conceptual difficulties inherent in the extension of thermodynamic

methods to far-from-equilibrium conditions. Consequently, simplified approximate models based on reasonable phenomenological assumptions are still an unavoidable step in the interpretation of hysteresis phenomena". This narration motived us to investigate the main reason behind voltage hysteresis generation in silicon anode half-cells. Wang et al. [8] at their work prepared self-healing silicon micro-particle anode based lithium-ion cell and conducted lithition-delithiation battery cycling test at four different C-Rates (C/10, C/5, C/3 & C/2). From the experimental results of battery cycling test for C/10, a huge voltage gap is witnessed (Figure-2.2(a))

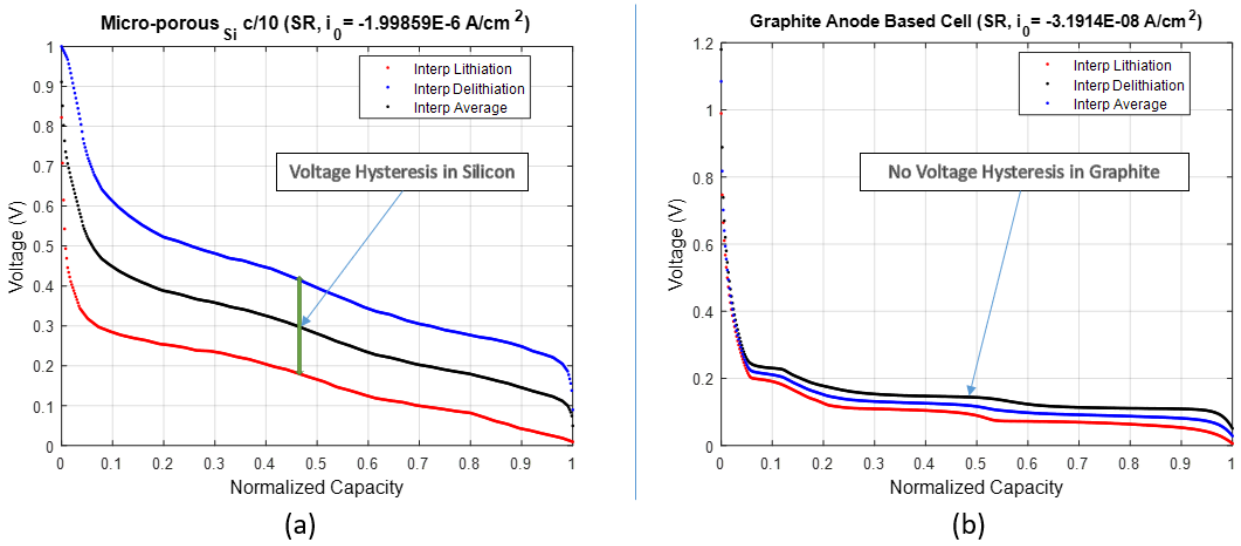

Figure-2.2: Identification of Voltage Hysteresis during lithiation-delithiation cycling in Silicon Anode based Lithium-Ion Batteries for C-Rate of C/10 (a) [8]; No voltage hysteresis is seen during battery cycling of Graphite Anode based Lithium-Ion Batteries for C-Rate of C/10 (b) [9]

In our lab, we experimented with commercial pouch cell where anode is made of traditional graphite as shown in Figure-2.2(b). In Figure-2.2(b) during battery cycling test of traditional lithium-ion batteries, no hysteresis has been witnessed. From the aforementioned observation, it is clear voltage hysteresis can be found in silicon anode which can eventually damage the battery. In

our work, we figured out the main reason behind this voltage hysteresis generation. We developed a physics-based mathematical model to predict this reason of voltage hysteresis generation.

2.3 Cracks Generation on Electrode Surface

Surface cracks generation during lithiation-delithiation cycling is another challenge which caught the attention of the battery scientists. The lifespan of silicon cells can be hampered highly if crack generation continuously occurs on the surface of the electrode. Particles can break into small pieces and eventually damage the battery.

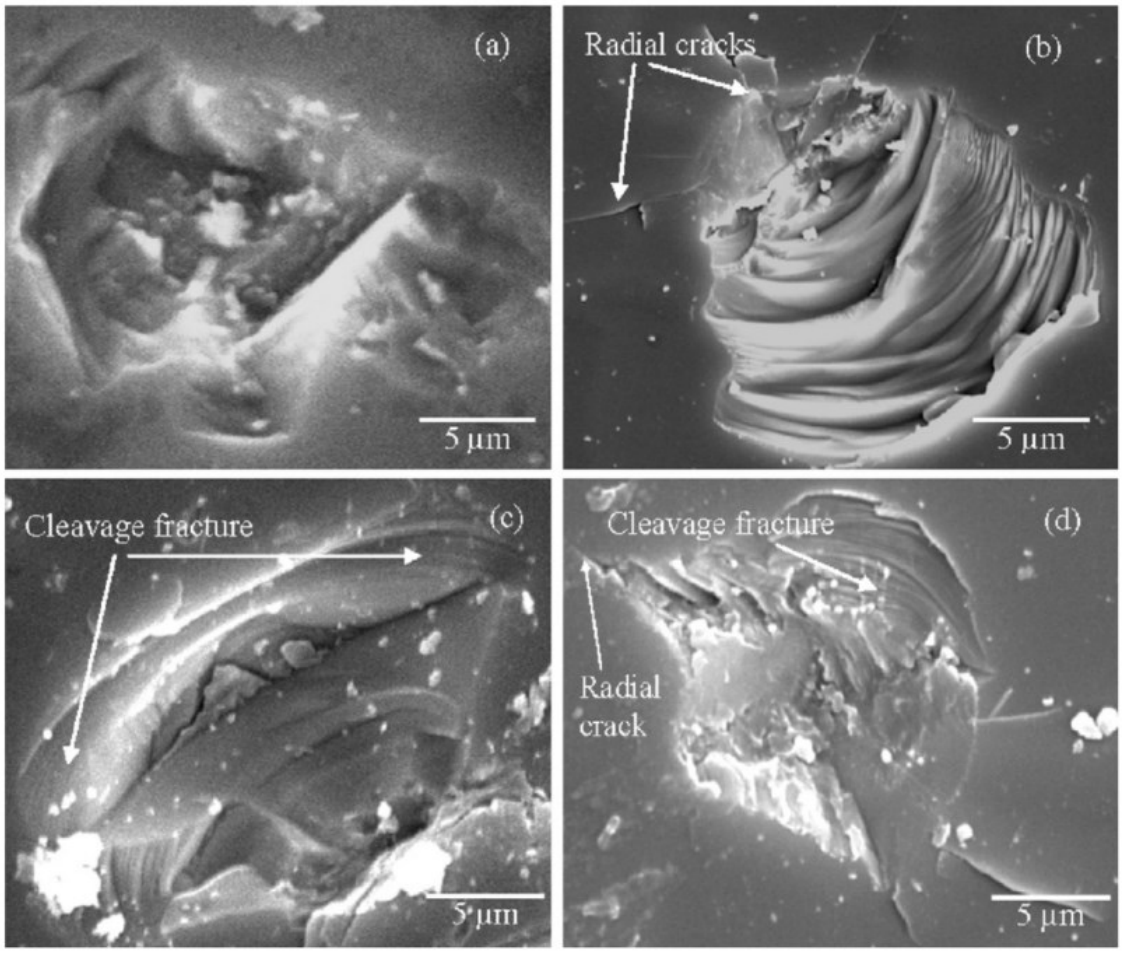

Figure-2.3: Representative crater impressions: crater with crushed zone (CC) (a), crater with crushed zone and radial cracks (CCR) (b), crater with crushed zone and brittle cleavage fractures (CCC) (c) and crater with crushed zone, brittle cleavage fractures and radial cracks (CCCR) (d). (Experiment parameters: 50 m alumina particle, 90◦ erosion angle, and 308 m/s particle striking velocity.) [12]

Different types of cracks formation are in line with the elastic–plastic material deformation have been presented by various researches [5,11–15]. In view of that, the SEM images shown in Figure-2.3 can be described as follows: (i) plastic indentation, but insufficient tensile stress to induce cracking [Figure-2.3(a)], (ii) radial and lateral cracking with some added features probably due to crystallography [Figure-2.3(b)], (c) primarily lateral cracking with minor radial cracks [Figure-2.3(c)], and (iv) radial and lateral cracking [Figure-2.3(d)]. All four figures show clear evidence of plastic indentation and crack generation.

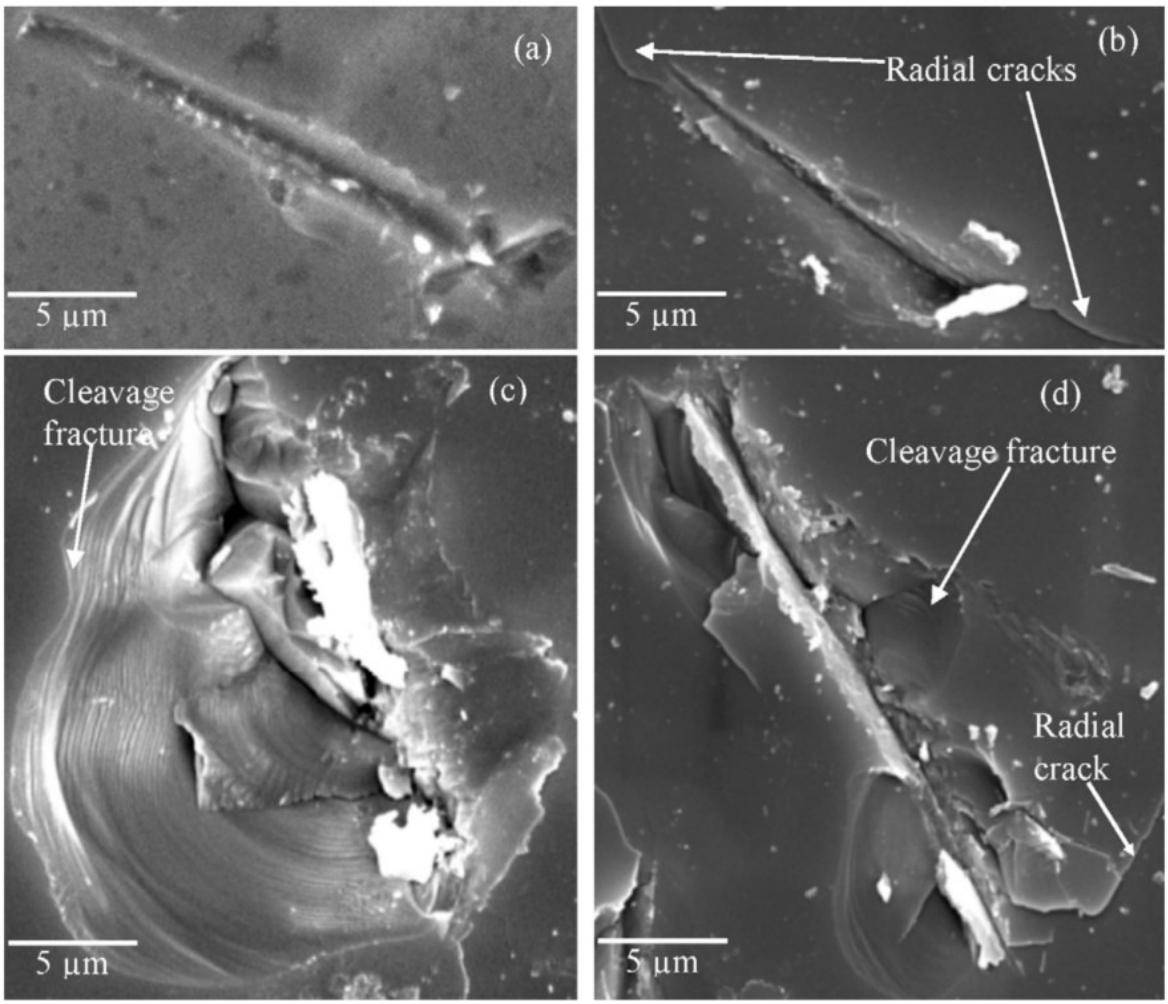

Figure- 2.4: Representative scratch impressions: scratch with crushed zone (SC) (a), scratch with crushed zone and radial cracks (SCR) (b), scratch with crushed zone and brittle cleavage fractures (SCC) (c) and scratch with crushed zone, brittle cleavage fractures and radial cracks (SCCR) (d). (Experiment parameters: 50 m alumina particle, 90◦ erosion angle, and 308 m/s particle striking velocity.) [12]

The only significant difference is in the extents of radial and lateral cracking. Likewise, as shown in Figure-2.4, the scratches can be further classified as (a) scratch with crushed zone (SC), (b) scratch with crushed zone and radial cracks (SCR) (c) scratch with crushed zone and brittle cleavage fractures (SCC) and (d) scratch with crushed zone, brittle cleavage fractures and radial cracks (SCCR). Figure-2.4 can also be explained according to elastic–plastic framework: starch without any cracking [Figure-2.4(a)], minor lateral cracking [Figure-2.4(b)], some radial cracking [Figure-2.4(c)], and considerable lateral cracking [Figure- 2.4(d], although much of the cracking failed to progress towards chip formation. Figures-2.3 and 2.4 are not fundamentally different, other than the impression shape. This is due to the fact that, alumina particles are irregular and one would expect a range of indentation zone (different width-to-length ratios) depending on the condition whether the particles strike the Si surface with a shape or blunt ends. As most scratches have a negligible depth, they are mainly responsible for crack network formation, which decreases material strength. These SEM images show how crucial surface crack generation can be. We have included this phenomena under in our battery model by implementing since as Li et al. [16] reported that the combined effect of lithium-ion diffusion, potential-concentration gradient and stress plays a crucial role in rate capability and cycle life of Si-based anodes of lithium ion batteries.

2.4 References

[1] D. Baker, M. Verbrugge, X. Xiao, An approach to characterize and clarify hysteresis phenomena of lithium-silicon electrodes, Journal of Applied Physics. 122 (2017) 165102. doi:10.1063/1.4995277.

[2] H. Wu, Y. Cui, Designing nanostructured Si anodes for high energy lithium ion batteries, Nano Today. 7 (2012) 414-429. doi:10.1016/j.nantod.2012.08.004.

[3] M. Verbrugge, D. Baker, X. Xiao, Q. Zhang, Y. Cheng, Experimental and Theoretical Characterization of Electrode Materials that Undergo Large Volume Changes and Application to the Lithium–Silicon System, The Journal of Physical Chemistry C. 119 (2015) 5341-5349. doi:10.1021/jp512585z.

[4] W. Zhang, A review of the electrochemical performance of alloy anodes for lithium-ion batteries, Journal of Power Sources. 196 (2011) 13-24. doi:10.1016/j.jpowsour.2010.07.020

[5] B. Boukamp, G. Lesh, R. Huggins, All-Solid Lithium Electrodes with Mixed-Conductor Matrix, Journal of The Electrochemical Society. 128 (1981) 725-729. doi:10.1149/1.2127495.

[6] M. Ashuri, Q. He, L. Shaw, Silicon as a potential anode material for Li-ion batteries: where size, geometry and structure matter, Nanoscale. 8 (2016) 74-103. doi:10.1039/c5nr05116a.

[7] G. Bertotti, I. Mayergoyz, V. Basso, A. Magni, Functional integration approach to hysteresis, Physical Review E. 60 (1999) 1428-1440. doi:10.1103/physreve.60.1428.

[8] C. Wang, H. Wu, Z. Chen, M. McDowell, Y. Cui, Z. Bao, Self-healing chemistry enables the stable operation of silicon microparticle anodes for high-energy lithium-ion batteries, Nature Chemistry. 5 (2013) 1042-1048. doi:10.1038/nchem.1802.

[9] A.A. Hossain, Y. Cha, M. Song, S.U. Kim, Side Reaction Correction and Non-linear Exchange Current Density for Mathematical Modeling of Silicon Anode Based Lithium-Ion Batteries, (2020). doi:10.13140/RG.2.2.36674.40646.

[10] Q. Wu, B. Shi, J. Bareño, Y. Liu, V. Maroni, D. Zhai et al., Investigations of Si Thin Films as Anode of Lithium-Ion Batteries, ACS Applied Materials & Interfaces. 10 (2018) 3487-3494. doi:10.1021/acsami.7b13980.

[11] M. McDowell, S. Lee, W. Nix, Y. Cui, 25th Anniversary Article: Understanding the Lithiation of Silicon and Other Alloying Anodes for Lithium-Ion Batteries, Advanced Materials. 25 (2013) 4966-4985. doi:10.1002/adma.201301795.

[12] A. Basak, J. Fan, J. Wang, P. Mathew, Material removal mechanisms of monocrystalline silicon under the impact of high velocity micro-particles, Wear. 269 (2010) 269-277. doi:10.1016/j.wear.2010.04.006.

[13] M. Gu, Y. He, J. Zheng, C. Wang, Nanoscale silicon as anode for Li-ion batteries: The fundamentals, promises, and challenges, Nano Energy. 17 (2015) 366-383. doi:10.1016/j.nanoen.2015.08.025.

[14] J. Christensen, J. Newman, A Mathematical Model of Stress Generation and Fracture in Lithium Manganese Oxide, Journal of The Electrochemical Society. 153 (2006) A1019. doi:10.1149/1.2185287.

[15] H. Sitinamaluwa, J. Nerkar, M. Wang, S. Zhang, C. Yan, Deformation and failure mechanisms of electrochemically lithiated silicon thin films, RSC Advances. 7 (2017) 13487-13497. doi:10.1039/c7ra01399j.

[16] J. Li, N. Dudney, X. Xiao, Y. Cheng, C. Liang, M. Verbrugge, Asymmetric Rate Behavior of Si Anodes for Lithium-Ion Batteries: Ultrafast Delithiation versus Sluggish Lithiation at High Current Densities, Advanced Energy Materials. 5 (2014) 1401627. doi:10.1002/aenm.201401627.

CHAPTER 3: LITERATURE SURVEY

3.1 Researches on Silicon in Wafers as Electrochemically Active Material

Before developing our own model, we performed a through literature survey. We wanted to check what types of experiment and modeling works are on-going with silicon anode in the battery arena. While there have been a lot of electrochemical studies on the silicon in wafers, the studies on silicon particles have been relatively. Some of the works on the silicon in wafers are highlighted below,

3.1.1 Experimental Research

3.1.1.1 Electrochemical Cell

Sethuraman et al. [1,2] fabricated electrode at their work using oxide free silicon wafers. Further, the Cu underlayer serves as a current collector, and aids in uniform current distribution on the Si electrode, an important role during the first cycle lithiation. The electrochemical-cell assembly is shown schematically in Figure-3.1.

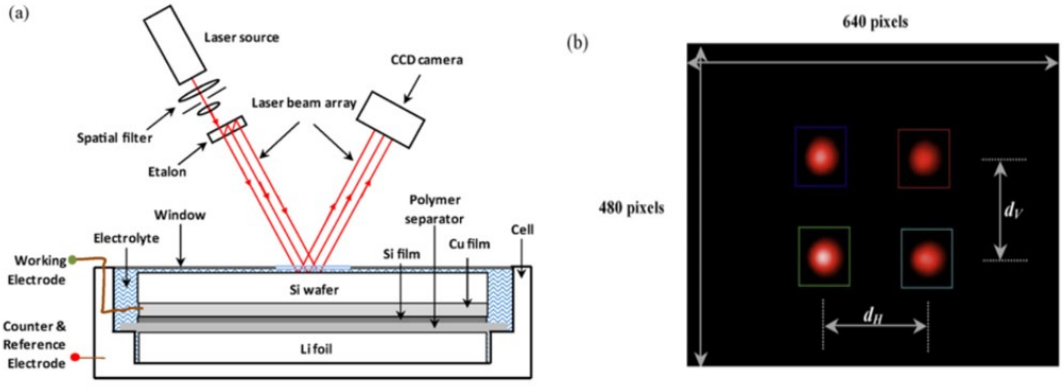

Figure- 3.1: Schematic illustration of the electrochemical-cell assembly; and the MOSS setup to measure substrate curvature (a). The relative change in the laser-spot spacing on the CCD camera's sensor is proportional to the curvature of the Si wafer (b). Note that the schematic is not drawn to scale. [1,2]

The Si wafer (coated with the Cu and Si thin films) was then assembled into a home-made electrochemical cell (Figure-3.1) with a lithium metal counter and reference electrode (diameter = 5.08 cm, thickness = 1.5 mm), and a woven Celgard 2500 separator (diameter = 5.2 cm, thickness = 50 m, Celgard Inc., Charlotte, NC). 1.2 M lithium hexafluoro phosphate in 1:2 (vol%) ethylene carbonate:diethyl carbonate with 10% fluoroethylene carbonate additive (Novolyte Technologies Inc., Independence, OH) was used as the electrolyte.

3.1.1.2 Electrochemical Measurements

The same group conducted electrochemical measurement in an environmental chamber. The cell was cycled galvanostatically at a current of 25 Acm^{-2} (ca. C/4 rate) between 1.2 [V] and 0.01 [V] vs. Li/Li^+. The lower limit of 0.01 [V] vs. Li/Li^+ was chosen to avoid lithium plating and to avoid the formation of the crystalline $Li_{15}S_4$ phase. Two open-circuit relaxation experiments were conducted at approximately 50% state of charge, one from the lithiation side and another from the delithiation side.

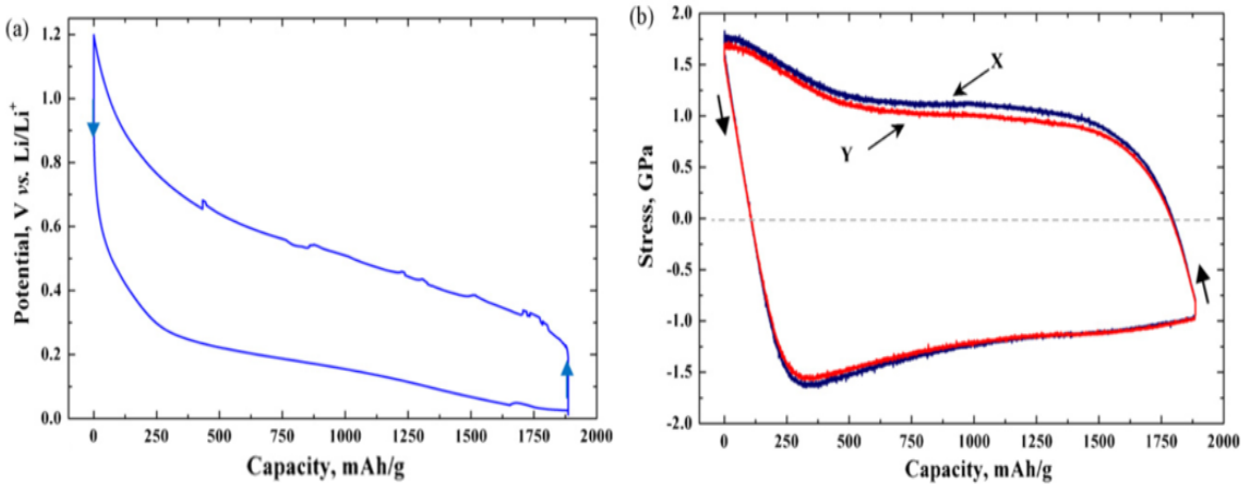

Figure-3.2: Cell potential vs. capacity curve corresponding to lithiation and delithiation of magnetron-sputtered amorphous Si thin-film electrode cycled at C/4 rate between 1.2 and 0.01 V vs. Li/Li^+ (a), and the corresponding stress calculated from the substrate curvature data using the Stoney equation (b). The curves labeled X and Y correspond to the stresses calculated from the averaged horizontal and the vertical displacement of the spots, respectively. The arrows in both figures indicate cycling direction. [1,2]

Then they conducted battery cycling test and observed the following experimental results [1,2]. Figure-3.2(a) shows battery cycling test results of wafer made Si anode-based LIBs. Voltage hysteresis is observed from their experiments as well. Whereas figure-3.2(b) exhibits stress [GPa] vs capacity [mAh/g] graph, which is calculated from Stoney's equation,

$$\sigma_f = \frac{E_s h_s^2 \kappa}{6 h_f (1-\nu_s)} \qquad [3.1]$$

An experimental investigation is carried out on silicon thin-film electrodes in which the stress is measured in situ during electrochemical lithiation and delithiation [1,2].

3.1.2 Modelling Development

Some researchers developed mathematical models and used Sethuraman et al.'s [1,2] experimental data to validate their model. A multi-physics microstructure-resolved model (MRM) has been developed by Wang et al. [4] for Li-ion battery (LIB) cells with an a-Si anode. The model couples the electrochemical kinetics, species transports, and structural/stress evolutions. The model was validated with experimental results in the literature.

Wang et al. developed a two-dimensional (2D) half-cell model and included two different parts at their model development, one is regarded as Sub-battery section and the other section is called Sub-stress. They used the experimental results as shown in Figure-3.2 from Sethuraman at el. [1,2]. Some of the simulation results of Wang et al. are shown is Figure-3.3. Other than them, few other groups [5-10] have also used the experimental data of Sethuraman et al. [1,2]. Here none of the group considered volumetric changes occurring in spherical silicon particles. Because of volume expansion, particle radius will also come into play. But nobody else has considered that.

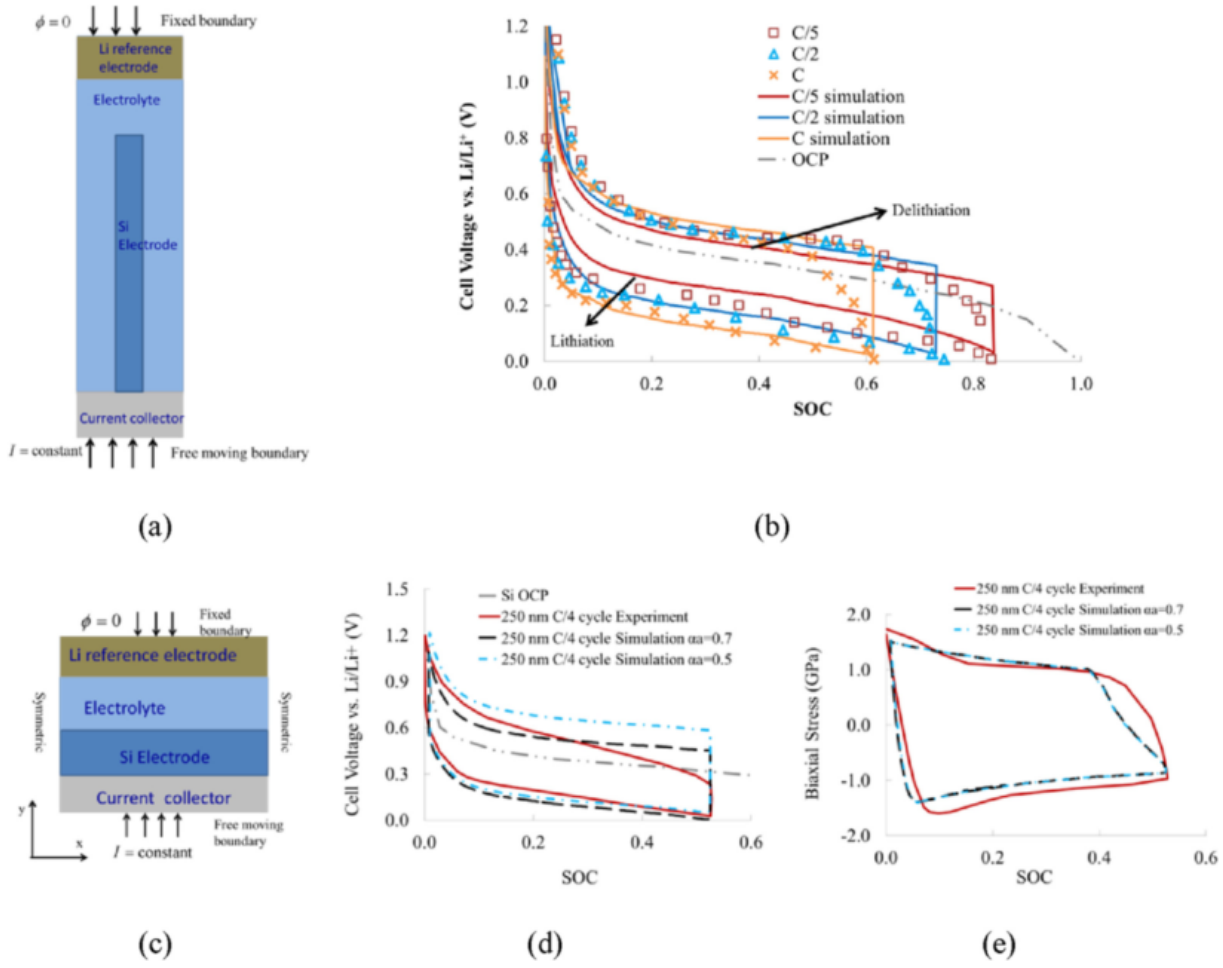

Figure-3.3: The schematic of cell model with Si nanowire (a). Comparisons of the cell voltage vs. SOC curves obtained by simulations with $k_0 = 8x10^{-15}$ (m/s) $(mol/m3)^{-0.7}$, $\alpha_a = 0.7$ and $\alpha_c = 0.3$ (solid lines) and the experimental results (markers) by Zhang et al. [18] (b). The FE model used to simulate of the experiment of the thin film a-Si electrode by Sethuraman et al. [2] (c). The comparison between simulations and experiments are given for both (d) cell voltage (d) and biaxial stress vs. SOC during cycling at C/4 rate (e). [4]

In our work, we gathered the data from actual silicon micro-particle cell used their data to validate our mathematical model. Two important factors, volume expansion and surface crack generation on the surface electrode were considered highly before developing our own model.

3.2 Researches on Spherical Particles of Silicon Anodes

3.2.1 Battery Modelling

Several battery researchers have developed models [4-15] to describe different kinds of physical phenomenon occurring inside batteries. But they did not consider physical challenges associated with silicon anodes such as volume expansion, crack generation on the surface electrode and particle size changing. Lacking in other researchers' [4-15] model motivated us to conduct more research on silicon anode.

3.2.1.1 Analytical Solution for Hydrostatic Stress

Hydrostatic stress is an important phenomenon in silicon anode. Earlier battery scientists said on the verdict that hydrostatic stress is the main reason behind voltage hysteresis. Cheng & Verbrugge [16] developed an analytical solution to calculate hydrostatic stress. The equation has been developed as below,

$$\sigma_h(R) = \frac{2E\Omega}{9(1-\nu)}[S_1 c_{av}(R) - c(R)] + S_2 \qquad [3.2]$$

This equation is dependent on molar concentration, c [mol/m^3] and average surface concentration c_{av} [mol/m^3]. Jin et al. [11] used this equation [4.1] at their work to calculate the stress-induced voltage. S_1 & S_2 can be calculated as,

$$S_1 = \frac{1 - \frac{K^S}{R_g}\frac{(1+\nu)}{E}}{1 + \frac{2K^S}{R_g}\frac{1-2\nu}{E}} \qquad [3.3]$$

$$S_2 = -\frac{\frac{2\tau^0}{R_g}}{1 + \frac{2K^S}{R_g}\frac{1-2\nu}{E}} \qquad [3.4]$$

K^s is regarded as Surface modulus [N/m] and τ^0 is denoted as Deformation independent surface tension [J/m]. R_g is known as the Universal gas constant [J/mol/K].

$$c_{av}(t) = c_0 + \frac{\int_0^t \frac{i_{app}(t)}{a_V FL}\,dt}{\epsilon a_V} = c_0 + \int_0^t \frac{i_{app}(t)}{\epsilon FL}\,dt \qquad [3.5]$$

Here, c_0 is the initial molar concentration [mol/m^3] and the other parameters are the same as before. A list of parameters has been added later in chapter-4.

3.2.1.2 Model Development without Volume Expansion and Experimental Validation

Jin et al. at their work developed a single particle spherical model. They included the analytical solution developed by Cheng and Verbrugge [16].

Instead of going with the traditional Butler-Volmer (BV) equation, they used a modified BV equation including hydrostatic stress induced voltage. The traditional Butler-Volmer (BV) equation is written as below [17],

$$j_n = \frac{i_0}{F}\left\{\exp\left[\frac{F(V-U)}{2RT}\right] - \exp\left[-\frac{F(V-U)}{2RT}\right]\right\} \qquad [3.6]$$

But Jin and his group [11] modified the above equation [4.2] as below,

$$j_n = \frac{i_0}{F}\left\{\exp\left[\frac{F(V-U)-\sigma_h\Omega}{2RT}\right] - \exp\left[-\frac{F(V-U)-\sigma_h\Omega}{2RT}\right]\right\} \qquad [3.7]$$

In the equation above, the stress induced voltage ($\sigma_h\Omega$) is included. Even though the group added this additional term in their model, they did not consider the volume expansion part in their model. The following equation is generally used to calculate this value,

$$i_0 = Fk_0 c_L^{1-\alpha}(c_{\max} - c_{\text{surf}})^{1-\alpha} c_{\text{surf}}^{\alpha} \quad [3.8]$$

Here, F is Faraday's constant [C/mol], k_0 is Rate constant. C_L is the concentration of electrolyte [mol/m^3]; c_{max} is the maximum concentration [mol/m^3] and c_{surf} is the surface concentration [mol/m^3] and α is the the net current density. Details about these equations have been discussed in chapter-4.

3.2.1.3 Stress Induced Diffusion

Zhang et al. [18] simulated intercalation-induced stresses during the discharge process and developed a stress-diffusion coupling model. They modified mass diffusion equation Fick's 2nd law as below,

$$\frac{\partial c}{\partial t} = D\frac{\partial}{\partial r}\left(\frac{\partial c}{\partial r} - \frac{\Omega c}{RT}\frac{\partial \sigma_h}{\partial r}\right) \quad [3.9]$$

Their boundary conditions were implemented as below,

$$D\left(\frac{\partial c}{\partial r} - \frac{\Omega c}{RT}\frac{\partial \sigma_h}{\partial r}\right) = -\frac{i_n}{F}\ ; when,\ r = R \quad [3.10]$$

$$D\left(\frac{\partial c}{\partial r} - \frac{\Omega c}{RT}\frac{\partial \sigma_h}{\partial r}\right) = 0\ ; when,\ r = 0 \quad [3.11]$$

From the equations above, hydrostatic stress was also calculated from the analytical solution of Cheng and Verbrugge [16]. Their simulations of spherical particles showed that larger

particle sizes and larger discharge current densities give larger intercalation induced stresses. Furthermore, internal stress gradients significantly enhance diffusion. In total, these results suggested that it is desirable to synthesize electrode particles with smaller sizes and larger aspect ratios to reduce intercalation-induced stress during the cycling of lithium-ion batteries.

Christensen et al. [19] incorporated a rigorous mathematical model for diffusion-induced stress generation in spherical Li-ion active materials into a full-cell model with porous electrodes. At their work, they showed that in conventional electrode materials (with small volume expansion), pressure diffusion plays a limited role in determining the galvanostatic voltage response but becomes important in determining the stress response, whereas variability in the solid-phase diffusion coefficient can have a significant impact on both the voltage and stress response. Pressure diffusion and nonlinear lattice expansion play an important role in determining both the voltage and stress response in large-volume-expansion materials (e.g., alloys and perhaps graphite at low utilization).

Stress evolution in cells with well-connected fragments exhibited up to three mechanical response regimes: rapid rise in stress within fragmented particles near the separator, stress increase in larger unfragmented particles once their concentration profiles become fully developed, and stress amplification in unfragmented particles due to the saturation of fragmented particles. Some of the results have been demonstrated on Figure-3.4. With the passage of time, stress tends to vary. Their results clearly indicate why it is so important to include stress in silicon anode-based battery model development. While developing our own model, we kept that one under our consideration.

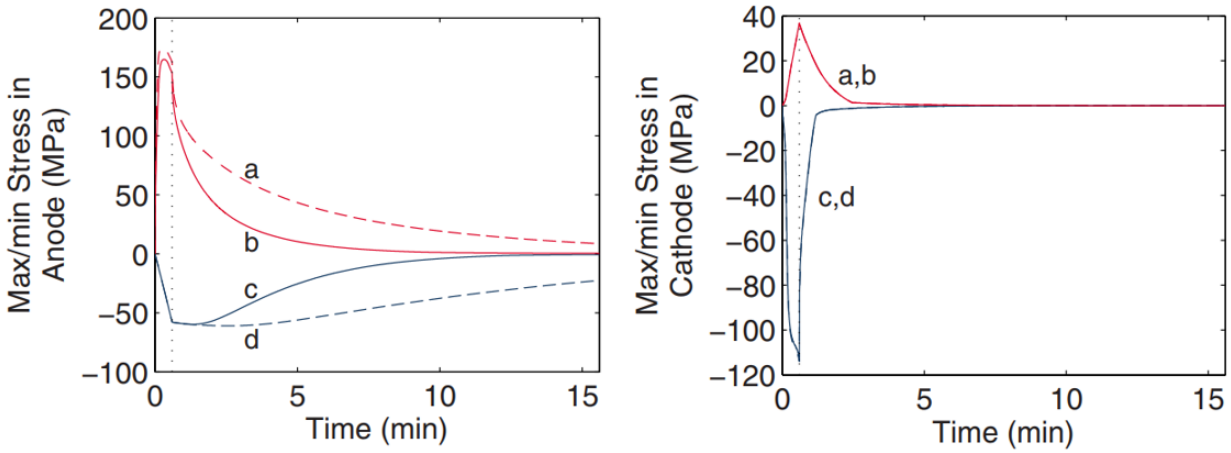

Figure-3.4: Color online stress extrema in an anode & cathode ("energy" cell) during a 36 s 10C discharge and subsequent relaxation. Maximum tangential stress (at particle surface), neglecting pressure diffusion (a); maximum tangential stress, including pressure diffusion (b); minimum radial and tangential stresses (at particle center), including pressure diffusion (c); and minimum radial and tangential stresses, neglecting pressure diffusion (d). The vertical dotted line indicates the time at which the current is interrupted. [19]

3.2.1.4 Single Particle Model

We wanted to make our model as simple as possible, therefore we have chosen to work with single particle one dimensional (1D) model. In the past, some researchers [11-13,20] worked with single particle model (SPM). But they overlooked important criteria. For example, Song et al. [12] and Jin et al. [11] worked with SPM, but they have not taken the volume expansion phenomenon into their account. Song [11] and Zhang [12] at the work theoretically investigated the effects of mechanical stresses on the voltage hysteresis of a lithium-ion battery during charge-discharge cycles. A diffusion-reaction-stress coupling model has been established. They found the voltage and overpotential are affected by diffusion-reaction-stress coupling. But they neither had experimental validation nor included volume changing part in their model which is a crucial part. Negligence of this part encouraged us to develop our own model.

3.2.2 Experimentation Work

We wanted to validate our mathematical model with experimental results. Therefore, we did some literature survey to find experimental research done with silicon anode-based lithium-ion batteries (LIBs). Some of the key results have been discussed in the following sections.

3.2.2.1 Asymmetric Diffusivity

Li et al. reported that the charging and discharging rates of lithium-ion-battery electrodes should be evaluated separately due to the asymmetric effect in the chemical in the chemical diffusion coefficients during lithiation and delithiation [21]. The following figure demonstrates the situation,

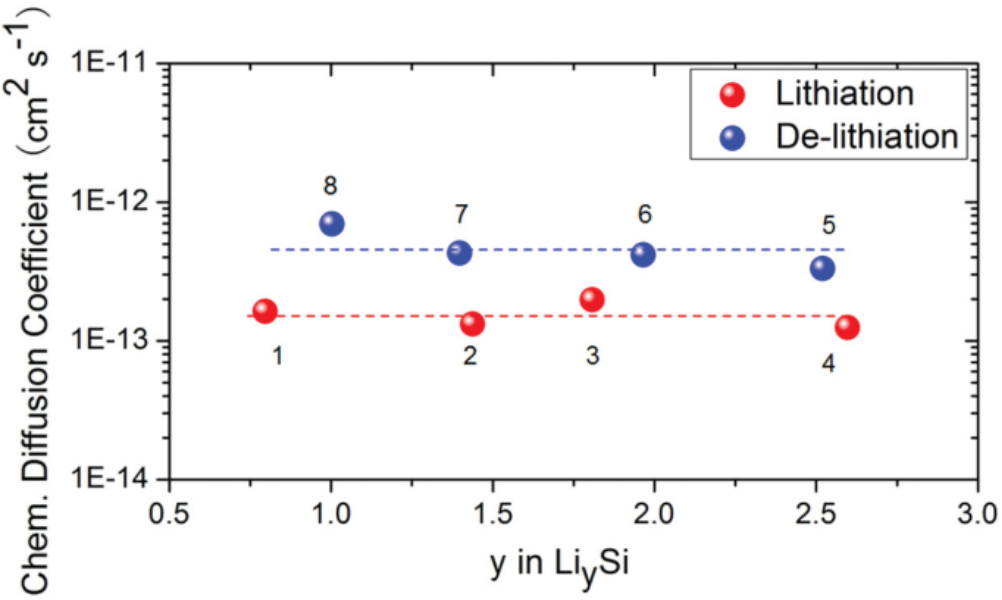

Figure-3.5: Chemical diffusion coefficients of Li in Si at different SOC values measured by PITT.[21]

From the figure, Diffusion coefficients have a smaller effect on the asymmetric rate performance, where the chemical diffusion coefficient in delithiation is approximately 3 times lower than that in lithiation. Their work provided new insight into determining the rate-limiting

component in lithium-ion batteries and identifying candidate electrodes for high-power applications. This part is very essential for model development.

3.2.2.2 Self-Healing Chemistry of Silicon Microparticles

Wang et al. [22] demonstrated self-healing chemistry of silicon active materials and conducted lithiation-delithiation cycling experiments at different C-Rates. They proceeded to fabricate the self-healing silicon electrodes by sealing SiMP's inside an SHP/CB composite coating. Coin cells with metallic lithium counter electrodes were employed to evaluate the electrochemical performance of the electrodes. On deep galvanostatic cycling between 0.01 [V] and 1 [V], the discharge (delithiation) capacity reached 2,617 [mAh/g] for the first cycle at a current density of 0.4 [A/g] which is about six times higher than the theoretical capacity of graphite. The electrode shows good cycling stability.

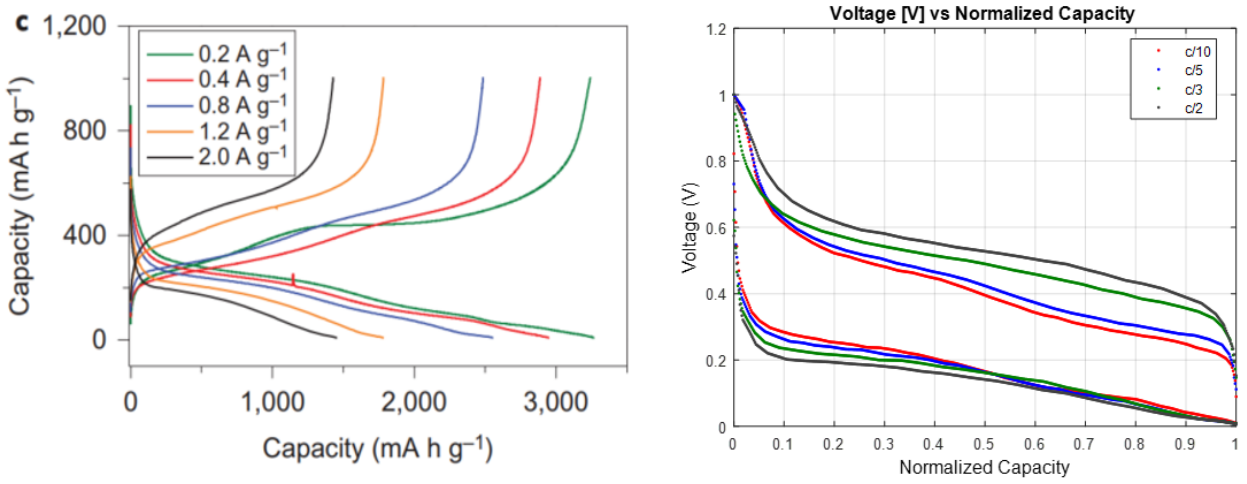

Figure-3.6: Cycling properties of the self-healing SiMP electrode (Capacity Retention) (a); Voltage vs Normalized Capacity for different C-Rates (C/10. C/5. C/3 & C/2) (b)[22]

Here, Rate-capability tests showed that the SiMP/SHP/CB electrodes retain their stable cycling stability at various rates, as shown (Figure-3.6(a)). Five different C-Rates such 0.2 A/g,

0.4 A/g, 0.8 A/g, 1.2 A/g and 2.0 A/g can be converted as C/20, C/10, C/5, C/3 and C/2 respectively. For both lithiation-delithiation cycling 3,200 [mAh/g] Capacity was achieved when the cycling test was conducting as C/20. Similarly, for C-Rates of C/10, C/5, C/3 and C/2, specific capacity was found as 2936.00 [mAh/g], 2544.48 [mAh/g], 1772.83 [mAh/g] and 1450.24 [mAh/g]. We used these experimental results to validate our mathematical model using simulation. Details have been provided in the next chapter.

Next, for experimental validation, we normalized the capacities by of each segment with a maximum capacity for four different C-Rates as C/10, C/5, C/3 and C/2. Then, we changed the direction of the current to create a complete battery cycling loop as shown in the Figure-3.6 (b).

3.2.2.3 Side-Reaction Correction

Side-reaction correction is another important factor. During battery cycling tests, some by-products are generated along with the main reaction at the interface of anode and separator. If by-products are not omitted, battery cycling loop cannot be completed. Therefore, it is necessary to rectify side reaction. Sethuraman et al. [23] demonstrated a technique to complete side-reaction.

According to them, If the marching behavior seen from cycle to cycle is caused by the electrolyte reduction reaction, the applied current during the lithiation process can then be written (ignoring double-layer charging) as:

Total current (i_{app}) = Lithiation current (i_{main}) + Electrolyte reduction current (i_{side}) [3.12]

Similar to the approaches taken by Darling and Newman [24] for the $Li_yMn_2O_4$ system and by Tafel and Newman [25] for the nickel hydroxide system, we assume Tafel kinetics for the electrolyte-reduction reaction. The current due to this reaction can be written as,

$$i_{side} = i_{0,SR} e^{\left[-\frac{\alpha_{side} F}{RT}(V - U_{side})\right]} \quad [3.13]$$

The transfer coefficient for the side reaction, α_{side}, was assumed to be 0.5. While Tafel kinetics does not provide an explicit equilibrium potential (i_o and U are related), Sethuraman et al. [23] assumed a value of U_{side}= 0.8 vs. Li/Li^+ to estimate $i_{0,SR}$. This side-reaction current was then calculated through the cycle assuming an i_0 such that the marching was eliminated from the cycling data. This is illustrated in Figures 3.7 and 3.8. Figure 3.7 shows the steady-state cycling data comprising of lithiation/delithiation cycle for C/10. Here it is noticed that initial and bottom points are not marching during the cycling test.

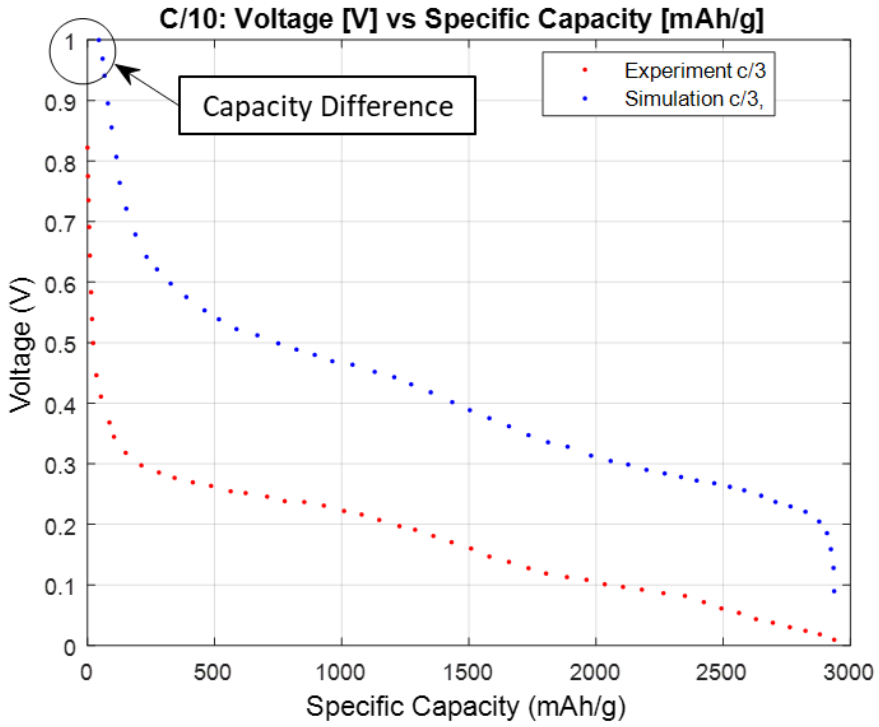

Figure-3.7: Voltage vs Normalized Capacity for C/10 (Without side-reaction correction) [22]

The voltage, V is collected from the experimental results. Here, F is denoted as Faraday's constant, F= 96485.3 [C/mol], R is gas constant, R = 8.314 [J/mol/K] and Temperature, T = 298 [K].

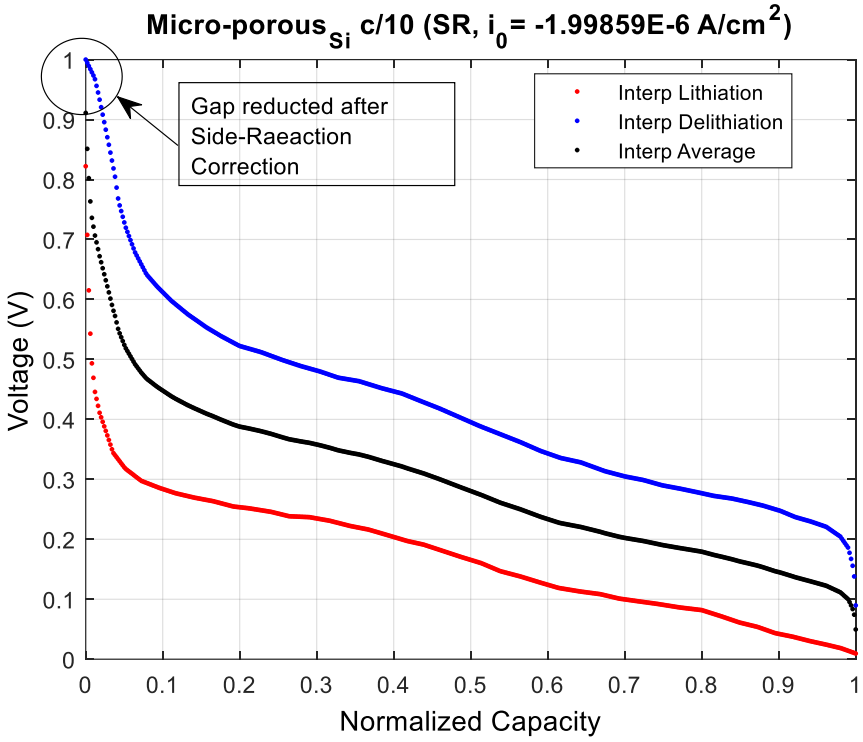

Figure-3.8: Voltage vs Normalized Capacity for C/10 (After side-reaction correction)

The figures above shown demonstrated how we implemented side-reaction correction on the experimental data of Want et al. [22]. It is necessary to get open circuit voltage (OCV) from the experiment. We used those data in our model.

3.3 References

[1] V. Sethuraman, M. Chon, M. Shimshak, V. Srinivasan, P. Guduru, In situ measurements of stress evolution in silicon thin films during electrochemical lithiation and delithiation, Journal of Power Sources. 195 (2010) 5062-5066. doi:10.1016/j.jpowsour.2010.02.013.

[2] V. Sethuraman, K. Kowolik, V. Srinivasan, Increased cycling efficiency and rate capability of copper-coated silicon anodes in lithium-ion batteries, Journal of Power Sources. 196 (2011) 393-398. doi:10.1016/j.jpowsour.2010.06.043.

[3] J. Maranchi, A. Hepp, A. Evans, N. Nuhfer, P. Kumta, Interfacial Properties of the a-Si/Cu:Active–Inactive Thin-Film Anode System for Lithium-Ion Batteries, Journal of The Electrochemical Society. 153 (2006) A1246. doi:10.1149/1.2184753.

[4] M. Wang, X. Xiao, X. Huang, A multiphysics microstructure-resolved model for silicon anode lithium-ion batteries, Journal of Power Sources. 348 (2017) 66-79. doi:10.1016/j.jpowsour.2017.02.037.

[5] V. Sethuraman, V. Srinivasan, A. Bower, P. Guduru, In Situ Measurements of Stress-Potential Coupling in Lithiated Silicon, Journal of The Electrochemical Society. 157 (2010) A1253. doi:10.1149/1.3489378.

[6] L. Baggetto, R.A.H. Niessen, F. Roozeboom, P.H.L. Notten, High energy density all-solid-state batteries: a challenging concept towards 3D integration, Adv.78 M. Wang et al./Journal of Power Sources 348 (2017) 66e79 Funct. Mater 18 (2008) 1057e1066. doi: 10.1002/adfm.200701245.

[7] J. Li, X. Xiao, F. Yang, M.W. Verbrugge, Y.-T. Cheng, Potentiostatic intermittent titration technique for electrodes governed by diffusion and interfacial reaction, J. Phys. Chem. C 116 (2012) 1472e1478. doi:10.1021/jp207919q.

[8] L. Baggetto, J.F.M. Oudenhoven, T. van Dongen, J.H. Klootwijk, M. Mulder, R.A.H. Niessen, M.H.J.M. de Croon, P.H.L. Notten, On the electrochemistry of an anode stack for all-solid-state 3D-integrated batteries, J. Power Sources 189 (2009) 402e410. doi.org/10.1016/j.jpowsour.2008.07.076.

[9] T. Swamy, Y.-M. Chiang, Electrochemical charge transfer reaction kinetics at the silicon-liquid electrolyte interface, J. Electrochem. Soc. 162 (2015) A7129eA7134. doi.org/10.1149/2.0181513jes.

[10] S. Pal, S.S. Damle, S.H. Patel, M.K. Datta, P.N. Kumta, S. Maiti, Modeling the delamination of amorphous-silicon thin film anode for lithium-ion battery, J. Power Sources 246 (2014) 149e159. doi.org/10.1016/j.jpowsour.2013.06.089

[11] C. Jin, H. Li, Y. Song, B. Lu, A. Soh, J. Zhang, On stress-induced voltage hysteresis in lithium ion batteries: Impacts of surface effects and inter-particle compression, Science China Technological Sciences. 62 (2019) 1357-1364. doi:10.1007/s11431-018-9491-6.

[12] Y. Song, A. Soh, J. Zhang, On stress-induced voltage hysteresis in lithium ion batteries: impacts of material property, charge rate and particle size, Journal of Materials Science. 51 (2016) 9902-9911. doi:10.1007/s10853-016-0223-y.

[13] B. Lu, Y. Song, Q. Zhang, J. Pan, Y. Cheng, J. Zhang, Voltage hysteresis of lithium ion batteries caused by mechanical stress, Physical Chemistry Chemical Physics. 18 (2016) 4721-4727. doi:10.1039/c5cp06179b.

[14] R. Deshpande, Y. Cheng, M. Verbrugge, Modeling diffusion-induced stress in nanowire electrode structures, Journal of Power Sources. 195 (2010) 5081-5088. doi:10.1016/j.jpowsour.2010.02.021.

[15] A. Bower, P. Guduru, V. Sethuraman, A finite strain model of stress, diffusion, plastic flow, and electrochemical reactions in a lithium-ion half-cell, Journal of The Mechanics And Physics Of Solids. 59 (2011) 804-828. doi:10.1016/j.jmps.2011.01.003.

[16] Y. Cheng, M. Verbrugge, The influence of surface mechanics on diffusion induced stresses within spherical nanoparticles, Journal of Applied Physics. 104 (2008) 083521. doi:10.1063/1.3000442.

[17] A. Latz, J. Zausch, Thermodynamic derivation of a Butler–Volmer model for intercalation in Li-ion batteries, Electrochimica Acta. 110 (2013) 358-362. doi:10.1016/j.electacta.2013.06.043.

[18] X. Zhang, W. Shyy, A. Marie Sastry, Numerical Simulation of Intercalation-Induced Stress in Li-Ion Battery Electrode Particles, Journal of The Electrochemical Society. 154 (2007) A910. doi:10.1149/1.2759840.

[19] J. Christensen, Modeling Diffusion-Induced Stress in Li-Ion Cells with Porous Electrodes, Journal of The Electrochemical Society. 157 (2010) A366. doi:10.1149/1.3269995.

[20] A.A. Hossain, Y. Cha, M. Song, S.U. Kim, Side Reaction Correction and Non-linear Exchange Current Density for Mathematical Modeling of Silicon Anode Based Lithium-Ion Batteries, (2020). doi:10.13140/RG.2.2.36674.40646.

[21] J. Li, N. Dudney, X. Xiao, Y. Cheng, C. Liang, M. Verbrugge, Asymmetric Rate Behavior of Si Anodes for Lithium-Ion Batteries: Ultrafast Delithiation versus Sluggish Lithiation at High Current Densities, Advanced Energy Materials. 5 (2014) 1401627. doi:10.1002/aenm.201401627.

[22] C. Wang, H. Wu, Z. Chen, M. McDowell, Y. Cui, Z. Bao, Self-healing chemistry enables the stable operation of silicon microparticle anodes for high-energy lithium-ion batteries, Nature Chemistry. 5 (2013) 1042-1048. doi:10.1038/nchem.1802.

[23] V. Sethuraman, V. Srinivasan, J. Newman, Analysis of Electrochemical Lithiation and Delithiation Kinetics in Silicon, Journal of The Electrochemical Society. 160 (2012) A394-A403. doi:10.1149/2.008303jes.

[24] R. Darling, J. Newman, Modeling Side Reactions in Composite $Li_yMn_2O_4$ Electrodes, Journal of The Electrochemical Society. 145 (1998) 990-998. doi:10.1149/1.1838376.

[25] K. Ta, J. Newman, Mass Transfer and Kinetic Phenomena at the Nickel Hydroxide Electrode, Journal of The Electrochemical Society. 145 (1998) 3860-3874. doi:10.1149/1.1838886.

CHAPTER 4: MATHEMATICAL MODEL

4.1 Model Development

4.1.1 Own Generated Mathematical Model

We wanted to make our model very simple. So, we started with a one-dimensional single spherical particle model. Following key features are added in our model,

- A physics-based mathematical model for silicon half-cell is generated.
- Single particle model is implemented.
- State of charge (SOC) dependent radius is used.
- Asymmetric diffusivity, D_s and exchange current density, i_0 values are used; one for lithiation cycle & the other for delithiation and specific volume is also changed as a function of radius.

We added a few mathematical equations which are necessary for model development. How we used them is explained in the following sections.

4.1.1.1 Governing Equations & Boundary Conditions

All the phenomenon happened inside the silicon anode has been represented by one single spherical particle. Fick's 2nd law known as mass diffusion equation can be presented as [1],

$$\frac{\partial c}{\partial t} = D\frac{\partial^2 c}{\partial r^2} + 2\frac{D}{r}\frac{\partial c}{\partial r} \qquad [4.1]$$

Here, c is denoted as Lithium concentration [mol/m^3]. D is regarded as Solid diffusivity [m^2/s] and r is the radius [m] working in the x-direction. t is denoted as time [s]. Two boundary conditions have been set. Boundary conditions & schematic diagram of the spherical particle are denoted as,

Boundary Condition-1 (BC-1):

$$D\frac{\partial c}{\partial r} = -\frac{i_{app}}{aVLF}\ ; for\ r = R \qquad [4.2]$$

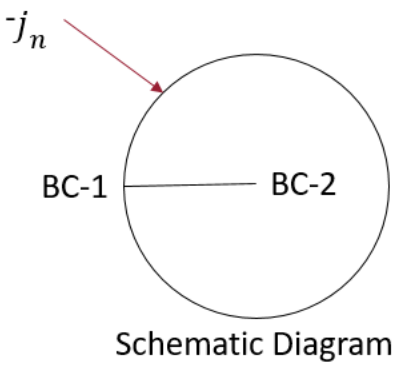

Boundary Condition-2 (BC-2):

$$D\frac{\partial c}{\partial r} = 0\ ; for\ r = 0 \qquad [4.3]$$

Here in the Boundary condition-1, j_n is the net flux [mol/m^2/s] it can be denoted as,

$$j_n = \frac{i_{app}}{aVLF} \qquad [4.4]$$

In the above equation, i_{app} is denoted as applied current [A/m^2], L is known as anode length [m]. F is Faradays' constant [C/mol]. aV is regarded as the surface-to-volume ratio [1/m], it is defined as below,

$$a = \frac{N * 4\pi R^2}{\frac{1}{\epsilon} N * \frac{4}{3}\pi R^3} = \frac{3\epsilon}{R} \qquad [4.5]$$

ε is denoted as porosity. N is the number of particles which is 1 in this case and R is the particle radius as a function SOC [m].

4.1.1.2 Auxiliary Conditions & Equations

4.1.1.2.1 Hydrostatic Stress

It was stated earlier, silicon particle experiences ~300% volume expansion during battery cycling and after several cycles crack generation occurs at the electrode surface. For this reason, hydrostatic stress develops during the cycling test. Verbrugge and Cheng [2] developed an

analytical solution for hydrostatic stress calculation. We included that stress term in our model. The equation has been developed as below,

$$\sigma_h(R) = \frac{2E\Omega}{9(1-\nu)}[S_1 c_{av}(R) - c(R)] + S_2 \qquad [4.6]$$

Here, σ_h is denoted as Hydrostatic stress [MPa]. E is known as Young's modulus [GPa]. ν is regarded as Poisson's ratio. Ω is Partial Molar Volume [m^3/mol]. c_{av}(R) is the average concentration influential for hydrostatic stress generation. The unit is [mol/m^3] and c(R) is the molar concentration at the surface. S_1 & S_2 is calculated as below,

$$S_1 = \frac{1 - \frac{K^S}{R_g}\frac{(1+\nu)}{E}}{1 + \frac{2K^S}{R_g}\frac{1-2\nu}{E}} \qquad [4.7]$$

$$S_2 = -\frac{\frac{2\tau^0}{R_g}}{1 + \frac{2K^S}{R_g}\frac{1-2\nu}{E}} \qquad [4.8]$$

We also discussed about these equations and in chapter no-3. Some of the parameters were used here has been in included in parameters list which will be discussed later.

Average surface concentration [mol/m^3] as a function of time is calculated developing following equation,

$$c_{av}(t) = c_0 + \frac{\int_0^t \frac{i_{app}(t)}{a_V FL}\,dt}{\epsilon a_V} = c_0 + \int_0^t \frac{i_{app}(t)}{\epsilon FL}\,dt \qquad [4.9]$$

Here, c_0 is the initial molar concentration [mol/m^3] and the other parameters are the same as before. A list of parameters has been added later in this chapter.

4.1.1.2.2 Modified Butler-Volmer (BV) Equation

For battery modeling, Butler-Volmer (BV) Equation is one of the most essential parts. Here we included the modified version of BV equation [3] where stress induced voltage part is included.

$$\frac{i_{app}}{a_V LF} = \frac{i_0}{F}\left\{\exp\left[(1-\alpha)\frac{F(V-U)-\sigma_h\Omega}{RT}\right] - \exp\left[-\alpha\frac{F(V-U)-\sigma_h\Omega}{RT}\right]\right\} \quad [4.10]$$

Here, $\sigma_h\Omega$ is called the stress induced voltage. Zhang et al. [4], Cheng and Verbrugge [2] and Jin et al. [1] all indicated how important it is to include this additional term in BV equation. i_0 is called the exchange current density. The following equation is generally used to calculate this value,

$$i_0 = Fk_0 c_L^{1-\alpha}(c_{\max} - c_{\text{surf}})^{1-\alpha} c_{\text{surf}}^{\alpha} \quad [4.11]$$

Where k_0 is known as Rate constant and c_{surf} & c_L are known as surface concentration [mol/m^3] & concentration of electrolyte [mol/m^3]. But, in our model, we used asymmetric exchange current density values instead of going with eqn [4.11]

Butler-Volmer equation can be derived as follow,

For lithium insertion into the silicon,

$$\text{LiSi} \rightarrow \text{Li}^+ + e^- + \text{Si} \quad [4.12]$$

The OCP, U can be expressed as

$$FU = \mu_{Li}^0 + \mu_{si} - \mu_{LiSi} \quad [4.13]$$

The electrochemical potential μ_{LiSi} can be expressed with the mechanical stress as

$$\mu_{LiSi} = \mu_{LiSi}^0 + RT\ln ax + \Omega\sigma_h \quad [4.14]$$

Where μ_0 is a constant value at reference state, R is the gas constant, T is the temperature, a is the activity coefficient, x is the mole fraction, and σ_h is hydrostatic stress. So,

$$FU = \mu_{Li}^0 + \mu_{si} - \mu_{LiSi}^0 - R_g T \ln ax - \Omega\sigma_h \quad [4.15]$$

Therefore, we may have shift in the OCP by the mechanical stress, and the OCP with mechanical stress, U_{st}

$$U_{st} = U + \frac{\Omega\sigma_h}{F} \quad [4.16]$$

Then, in the cell-level modeling, this can be included in the Butler-Volmer equation:

$$j_n = \frac{i_0}{F}\left\{\exp\left[(1-\alpha)\frac{F(V-U)-\sigma_h\Omega}{RT}\right] - \exp\left[-\alpha\frac{F(V-U)-\sigma_h\Omega}{RT}\right]\right\} \quad [4.17]$$

If the symmetric coefficient $\alpha = 1/2$

$$\frac{j_n F}{2i_0} = \sinh\frac{F(V-U)-\sigma_h\Omega}{2RT} \quad [4.18]$$

Or

$$V = U + \frac{\sigma_h\Omega}{\mathrm{F}} + \frac{2R_g T}{F}\operatorname{asinh}\frac{j_n F}{2i_0} \quad [4.19]$$

Putting the value of flux value j_n the above equation can be written as,

$$V = U + \frac{\sigma_h\Omega}{\mathrm{F}} + \frac{2R_g T}{F}\sinh^{-1}\left(\frac{i_{app}}{2i_0 a\, LF}\right) \quad [4.20]$$

Here, V is the Voltage [V] and other parameters have been discussed. We used this equation no [4.19] in our model to generate several results.

4.1.1.2.3 Radius as a Function of State of Charge (SOC)

This is the most important feature of our model. As it was mentioned earlier silicon particle experiences ~300% expansion during lithiation and contraction during delithiation. Therefore, the radius of the particle also experiences a change of radius as the state of charge (SOC) progresses. Derivation of particle radius has been discussed here.

When the particle is fully delithiated, the SOC is 0, we considered the particle volume as $V = V_0$. Since, silicon experiences ~300% volume expansion during lithiation. At fully lithiatied condition, when SOC=1, Final particle volume becomes as $V = 3V_0$.

Since, we are considering spherical particle. Therefore, we considered volume equation as $V = \frac{4}{3}\pi r^3$. Following schematic diagram shows the working principle,

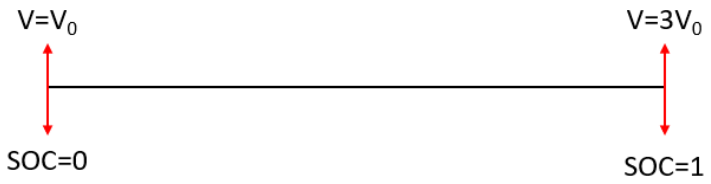

Here, When SOC = 0, $V_i = V_0$ and at SOC =1, $V_f = 3V_0$

The volume equation is developed as below,

$V(SOC) = V_0 + SOC(V_f - V_i)$

$\Rightarrow V(SOC) = V_0 + SOC(3V_0 - V_0)$ [At fully lithiated state]

$\Rightarrow V(SOC) = V_0 + SOC(2V_0)$

$\Rightarrow V(SOC) = V_0(1 + 2SOC)$

$\Rightarrow \frac{4}{3}\pi r^3(SOC) = \frac{4}{3}\pi r_0^3(1 + 2SOC)$

$$r(SOC) = r_0\sqrt[3]{(1 + 2SOC)}$$

Therefore, our own developed equation can be written as below,

$$r(SOC) = r_0[1 + (2SOC)]^{\frac{1}{3}} \qquad [4.21]$$

Here, r_0 is defined as initial particle radius. SOC is regarded as the State of Charge. r(SOC) is defined as the particle radius equation as a function of SOC. We are the first one to include this feature in mathematical battery model development.

How volume and particle radius are connected with SOC has been discussed in the section below,

The following figure demonstrates how does it work as SOC changes.

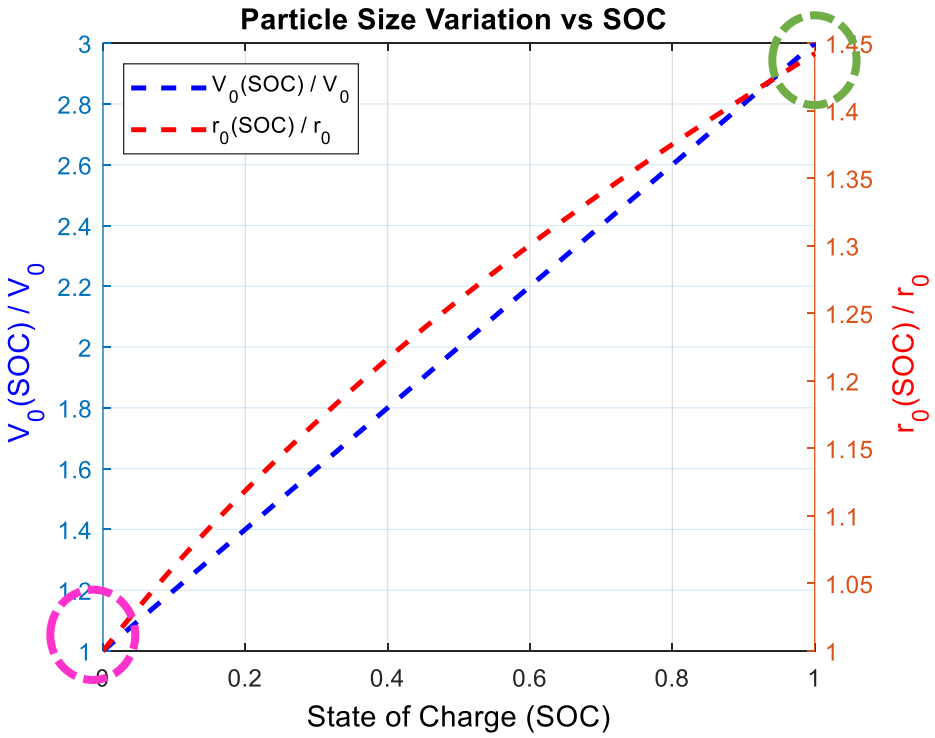

Figure-4.1: Working Principle of Particle Radius as a Function of SOC

The following table explains how equation [4.12] is developed,

Circle	SOC	State	$\frac{v_0(SOC)}{v_0}$	$\frac{r(SOC)}{r_0}$
Pink	0	Unlithiated	1	1
Green	1	Fully lithiated	3	1.45

In Figure-4.1, the pink circle denotes unlithiated condition when SOC is 0 and the green circle denotes fully lithiated condition when SOC=1. State of charge is defined as below,

$$SOC = \frac{Avergae\ Concentration}{Maximum\ Concentration} = \frac{c_{avg}}{c_{\max}} \qquad [4.22]$$

At unlithiated condition, the volume is constant and defined as 1. As SOC progresses, volume keeps increasing, and at fully lithiated condition particle experiences ~300% volume expansion meaning volume enlarges 3 times the initial volume. Therefore, at fully lithiated condition, the ratio of $v_0(SOC)/v_0$ becomes 3.

Similarly, $r_0(SOC)/r_0$ is 1 at unlithiated condition and as SOC progress when SOC becomes 1, the particle radius ratio becomes 1.45.

4.1.1.2.4 Asymmetric Solid Diffusivity

Another new feature we added in our model is the usage of asymmetric solid diffusivity. In the past, previous researchers used constant value throughout the model. Since Li et al. [5] reported at their work, charging and discharging rates of lithium-ion-battery electrodes should be evaluated separately due to the asymmetric effect in the chemical in the chemical diffusion

coefficients during lithiation and delithiation. Therefore, we used two different values for solid diffusivity, one for lithiation and another one for delithiation instead of going with constant values throughout. Results have been demonstrated in the following chapter.

4.1.1.2.5 Asymmetric Exchange Current Density

Likewise, asymmetric solid diffusivity, for the case of exchange current density we used two different exchange current density values one for lithiation and another one for delithiation. In general case eqn [4.11] is commonly used by most researchers. In our case, we used asymmetric values as Li et al. at their report [5] provided new insight into determining the rate-limiting component in lithium-ion batteries and identifying candidate electrodes for high-power applications. We are the first one in this field to include these crucial features in modelling development.

4.1.1.3 Merging of Single Particle Model, Stress & Strain, Stress-Induced Diffusion, Volume Expansion and Asymmetric Parameters

In our model work we merged single particle model (SPM), included mass diffusion equation (Fick's law), hydrostatic stress induced Butler-Volmer (BV) equation, volume expansion, state of charge (SOC) based particle radius, asymmetric diffusivity and asymmetric exchange current density all together and developed our physics-based mathematical model. We set two boundary conditions as discussed earlier. One at the center of the particle and other one at the surface of the spherical particle. The following Band-Map model will highlight the key equations we included in our model.

Table-4.1: Governing equations and boundary conditions for the SPM model.

Governing Equations	Boundary Conditions
Mass Balance in Solid Phase (spherical coordinate) (c_s: lithium concentration), $\frac{\partial c}{\partial t} = D\frac{\partial^2 c}{\partial r^2} + 2\frac{D}{r}\frac{\partial c}{\partial r}$	$D\frac{\partial c}{\partial r}\|_{r=R} = -\frac{i_{app}}{a\,LF}; \quad D\frac{\partial c}{\partial r}\|_{r=0} = 0$
Average Concentration Profile in Solid Phase, $\epsilon FL\frac{dc_{av}(t)}{dt} = i_{app}(t)$	
Modified Butler-Volmer Voltage Equation, $V = U + \frac{\sigma_h \Omega}{\mathrm{F}} + \frac{2RT}{F}\sinh^{-1}\left(\frac{i_{app}}{2i_0 a\,LF}\right)$	

In order to find the parameters, we did some literature survey and identified the best parameters required to compile our model. The parameters we used in our model is given below,

Table-4.2: List of model parameters used in this study

Parameters	Values	Description	Remarks
r_0	2.1 x 10^{-6}	Initial Particle Radius [m]	Ref [7]
D_l	2 x 10^{-15}	Solid Diffusivity [m^2/s] for Lithiation	Measured
D_d	5 x 10^{-15}	Solid Diffusivity [m^2/s] for Delithiation	
$\hat{C}$	Calculated from experiment	Columbic Capacity [mAh/g]	"

i_{0l}	0.006	Exchange Current Density [A/m^2] for Lithiation	“
i_{0d}	0.008	Exchange Current Density [A/m^2] for Delithiation	“
c_{max}	$\rho \times \frac{\hat{C}}{F}$	Maximum Concentration [mol/m^3]	“
C-rate	Calculated from experiment	C-Rate [1/h]	“
c_{01}	$x_0 \times c_{max}$	Initial Concentration [mol/m^3]	Ref [1]
E	90	Young's Modulus Constant [GPa]	Ref [6]
v	0.28	Poisson's Ratio Constant	“
ε	0.6517	Volume Ratio of Silicon	“
L	116 x 10^{-6}	Thickness of Electrode [m]	Ref [1]
F	96487	Faraday Constant [C/mol]	“
R_g	8.314	Universal Gas Constant [J/mol/K]	“
T	298	Temperature [K]	“
ρ	2330	Density of Silicon [kg/m^3]	“
x_0	0.0001	Initial SOC of silicon 0.0001	“
Ω	4.5 x 10^{-6}	Partial Molar Volume [m^3/mol]	Ref [6]
K^s	5	Surface Modulus [N/m]	Ref [2]
τ_0	1	Deformation-Independent Surface Tension [J/m^2]	“
m	1.043798 x 10^{-3}	Mass of the Cell [kg]	Measured

4.1.2 Discussion

As we mentioned before we wanted to make our model as simple as possible. Therefore, we started with a single spherical particle one-dimensional model. The extra features we have in our model is volume expansion, variable radius as a function of SOC, asymmetric diffusivity and asymmetric exchange current density, modified Butler-Volmer (BV) equation having hydrostatic stress induced voltage term. After developing the model, we ran a simulation in COMSOL Multiphysics 5.5 and validated our model with experimental data from Wang et al. [7]. Details have been provided in the following chapter.

4.2 References

[1] A.A. Hossain, Y. Cha, M. Song, S. U. Kim, Side Reaction Correction and Non-linear Exchange Current Density for Mathematical Modeling of Silicon Anode Based Lithium-Ion Batteries, (2020). doi:10.13140/RG.2.2.36674.40646.

[2] Y. Cheng, M. Verbrugge, The influence of surface mechanics on diffusion induced stresses within spherical nanoparticles, Journal of Applied Physics. 104 (2008) 083521. doi:10.1063/1.3000442.

[3] C. Jin, H. Li, Y. Song, B. Lu, A. Soh, J. Zhang, On stress-induced voltage hysteresis in lithium ion batteries: Impacts of surface effects and inter-particle compression, Science China Technological Sciences. 62 (2019) 1357-1364. doi:10.1007/s11431-018-9491-6.

[4] X. Zhang, W. Shyy, A. Marie Sastry, Numerical Simulation of Intercalation-Induced Stress in Li-Ion Battery Electrode Particles, Journal of The Electrochemical Society. 154 (2007) A910. doi:10.1149/1.2759840.

[5] J. Li, N. Dudney, X. Xiao, Y. Cheng, C. Liang, M. Verbrugge, Asymmetric Rate Behavior of Si Anodes for Lithium-Ion Batteries: Ultrafast Delithiation versus Sluggish Lithiation at High Current Densities, Advanced Energy Materials. 5 (2014) 1401627. doi:10.1002/aenm.201401627.

[6] S. Pal, S.S. Damle, S.H. Patel, M.K. Datta, P.N. Kumta, S. Maiti, Modeling the delamination of amorphous-silicon thin film anode for lithium-ion battery, J. Power Sources 246 (2014) 149e159. doi.org/10.1016/j.jpowsour.2013.06.089.

[7] C. Wang, H. Wu, Z. Chen, M. McDowell, Y. Cui, Z. Bao, Self-healing chemistry enables the stable operation of silicon microparticle anodes for high-energy lithium-ion batteries, Nature Chemistry. 5 (2013) 1042-1048. doi:10.1038/nchem.1802.

CHAPTER 5: RESULTS AND DISCUSSION

5.1 Sensitivity Analysis

From our model, we identified some key parameters as solid diffusivity (D_s), exchange current density (i_0), partial molar volume (Ω), Young's modulus (E) and Poisson's ratio (ν). These parameters play a crucial role in experimental validation with our model. To find the best fit with experimental results we need to choose the most suitable parametric values. Therefore, before running simulations, we conducted some literature surveys and figured out the best parametric ranges.

First, we figured out five different values of solid diffusivity for the lithiation cycle. For experimental validation, we choose experimental data of four (4) different C-Rates (C/10, C/5, C/3 and C/2) generated by Wang et al [1]. Once we figured out the best value from literature surveying [2-9], we selected parametric ranges. Then, within the parameter values, we selected one particular value for simulation and repeated the same technique with solid diffusivity for delithiation cycle. Next, we repeated the same procedure for the exchange current density for lithiation cycle and then repeated the same for delithiation cycle. Once we find good values, then we moved to other key parameters such as Ω, E and ν.

After completing sensitivity analysis, we generated voltage vs specific capacity, hydrostatic stress vs specific capacity and stress induced voltage vs specific capacity graphs for four different types of C-Rates. In the following section, details have been provided.

5.1.1 Impact of Solid Diffusivity

5.1.1.1 Lithiation Cycle

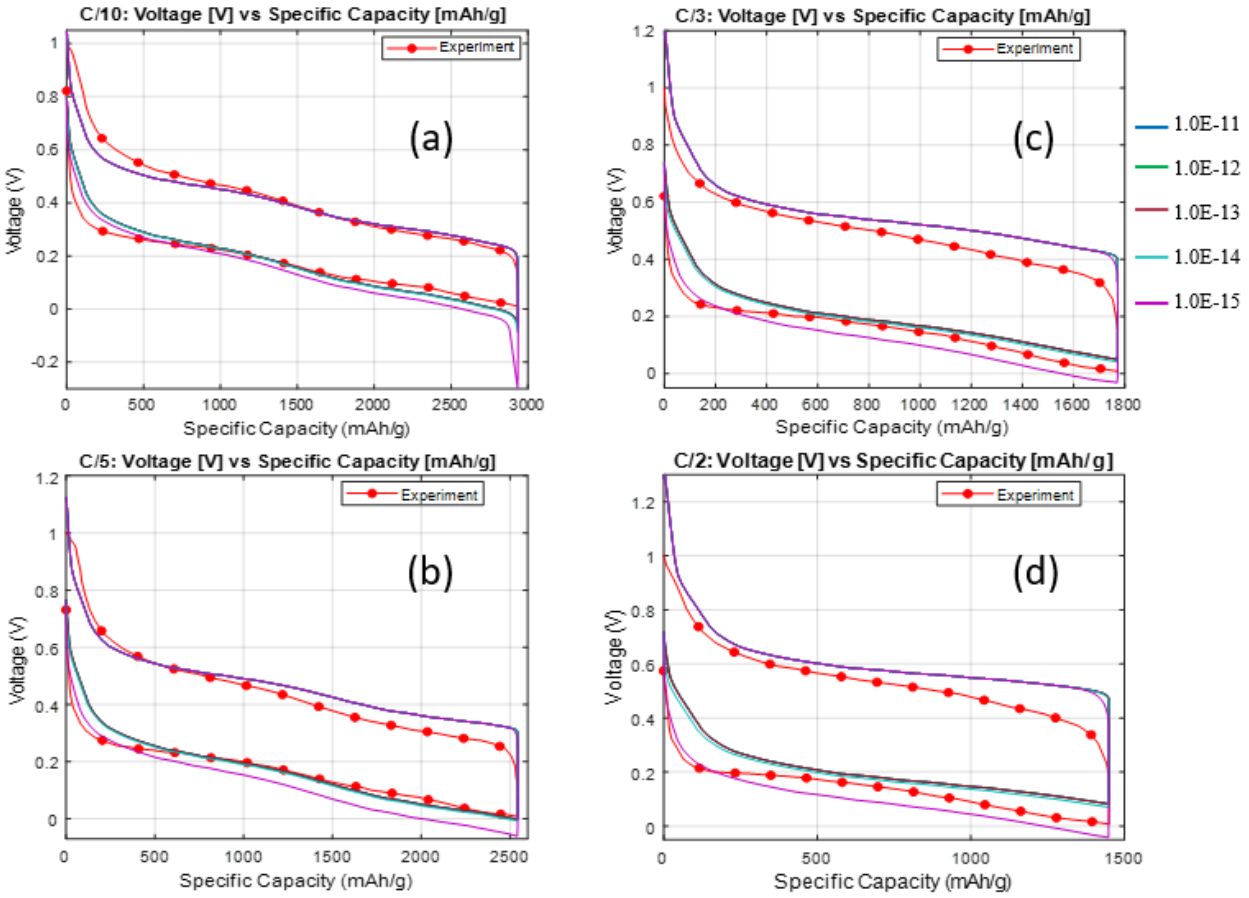

Figure-5.1: Sensitivity analysis in voltage vs specific capacity graph for different solid diffusivity in lithiation cycle. Results of different C-Rates: C/10 (a), C/5 (b), C/3 (c), C/2 (d) have been demonstrated.

Table-5.1: Parametric ranges for sensitivity analysis of solid diffusivity (d_l) in lithiation cycle

Solid Diffusivity [m^2/s] values used in Lithiation Cycle				
1.0E-11	1.0E-12	1.0E-13	1.0E-14	1.0E-15

At table-5.1 the different diffusivity values which we used in simulation has been highlighted. The best-fitting value we found so far is D_l = 2.0E-15 [m^2/s].

5.1.1.2 Delithiation Cycle

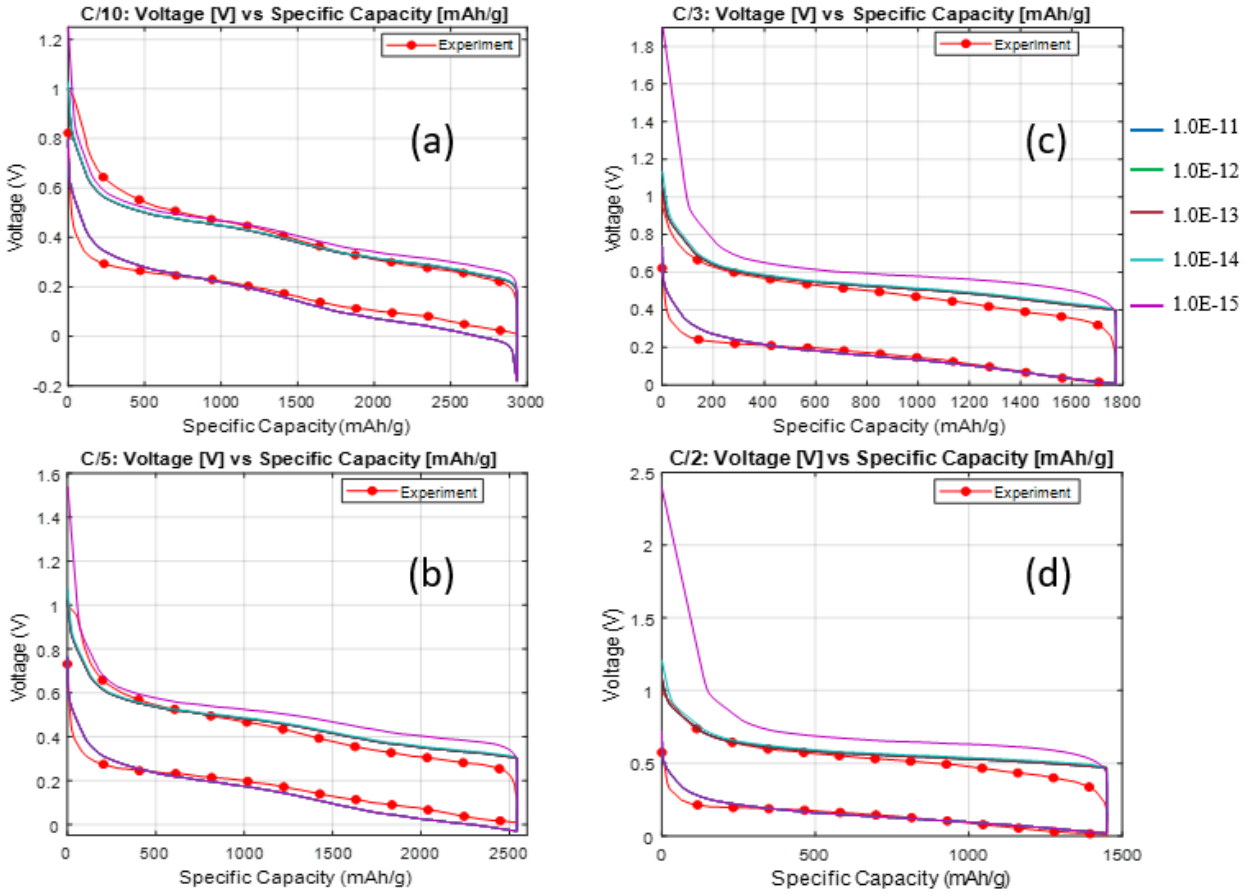

Figure-5.2: Sensitivity Analysis in Voltage vs Specific Capacity graph for different Solid Diffusivity in Delithiation cycle. Results of different C-Rates: C/10 (a), C/5 (b), C/3 (c) C/2 (d) have been demonstrated.

Table-5.2: Parametric ranges for sensitivity analysis of solid diffusivity (d_d) in delithiation cycle

Solid Diffusivity [m^2/s] values used in Delithiation Cycle				
1.0E-11	1.0E-12	1.0E-13	1.0E-14	1.0E-15

Here, table-5.2 the different diffusivity values which we used in simulation have been shown. The best-fitting value is D_d = 5.0E-15 [m^2/s].

5.1.2 Impact of Exchange Current Density

5.1.2.1 Lithiation Cycle

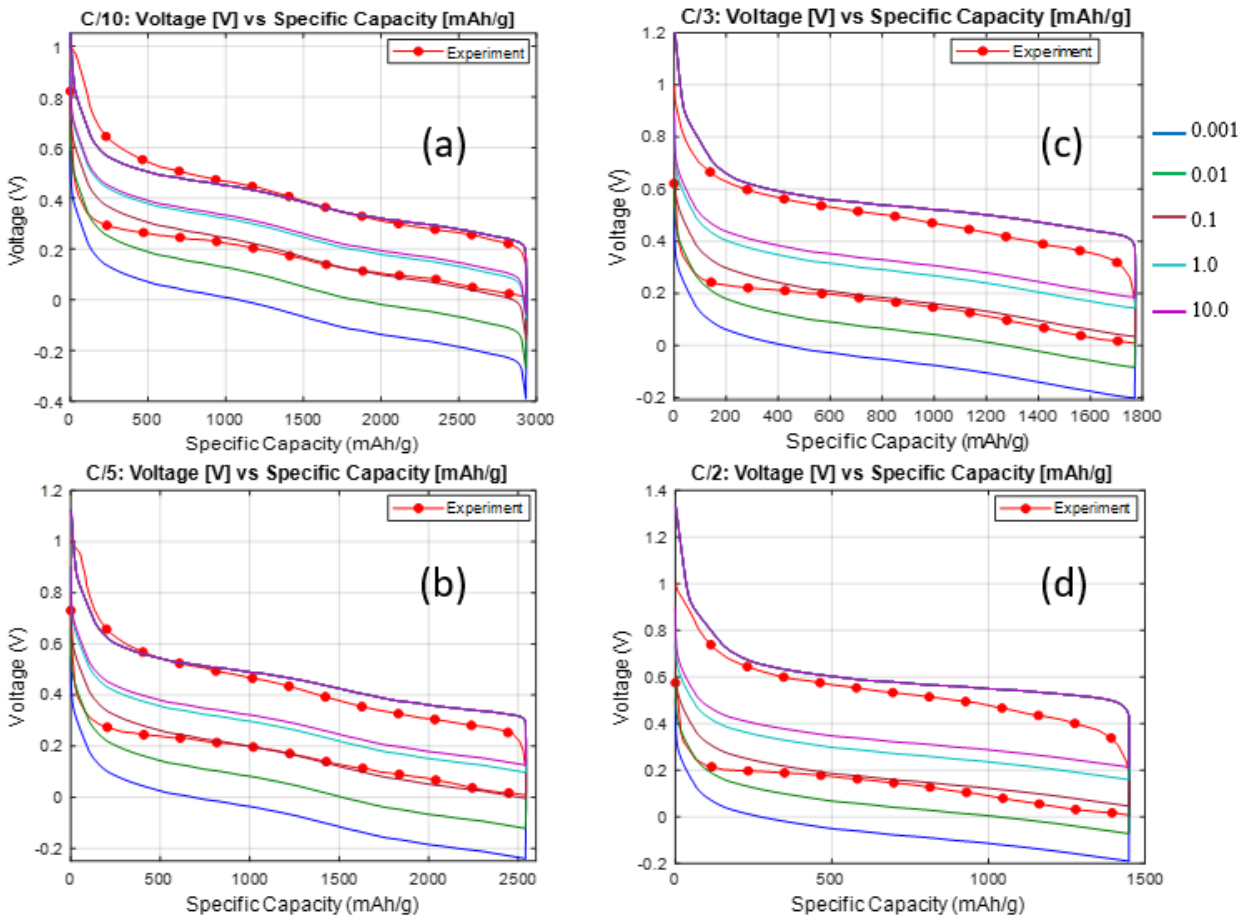

Figure-5.3: Sensitivity Analysis in Voltage vs Specific Capacity graph for different Exchange Current Density in lithiation cycle. Results of different C-Rates: C/10 (a), C/5 (b), C/3 (c), C/2 (d) have been demonstrated.

Table-5.3: Parametric ranges for sensitivity analysis of exchange current density ($i0_l$) in lithiation cycle

Exchange Current Density [A/m^2] values used in Lithiation Cycle				
0.001	0.01	0.1	1.0	10.0

At table-5.3 the different exchange current density values which we used in simulation has been exhibited. The best-fitting value we got here is $i0_l = 0.06$ [A/m^2].

5.1.2.2 Delithiation Cycle

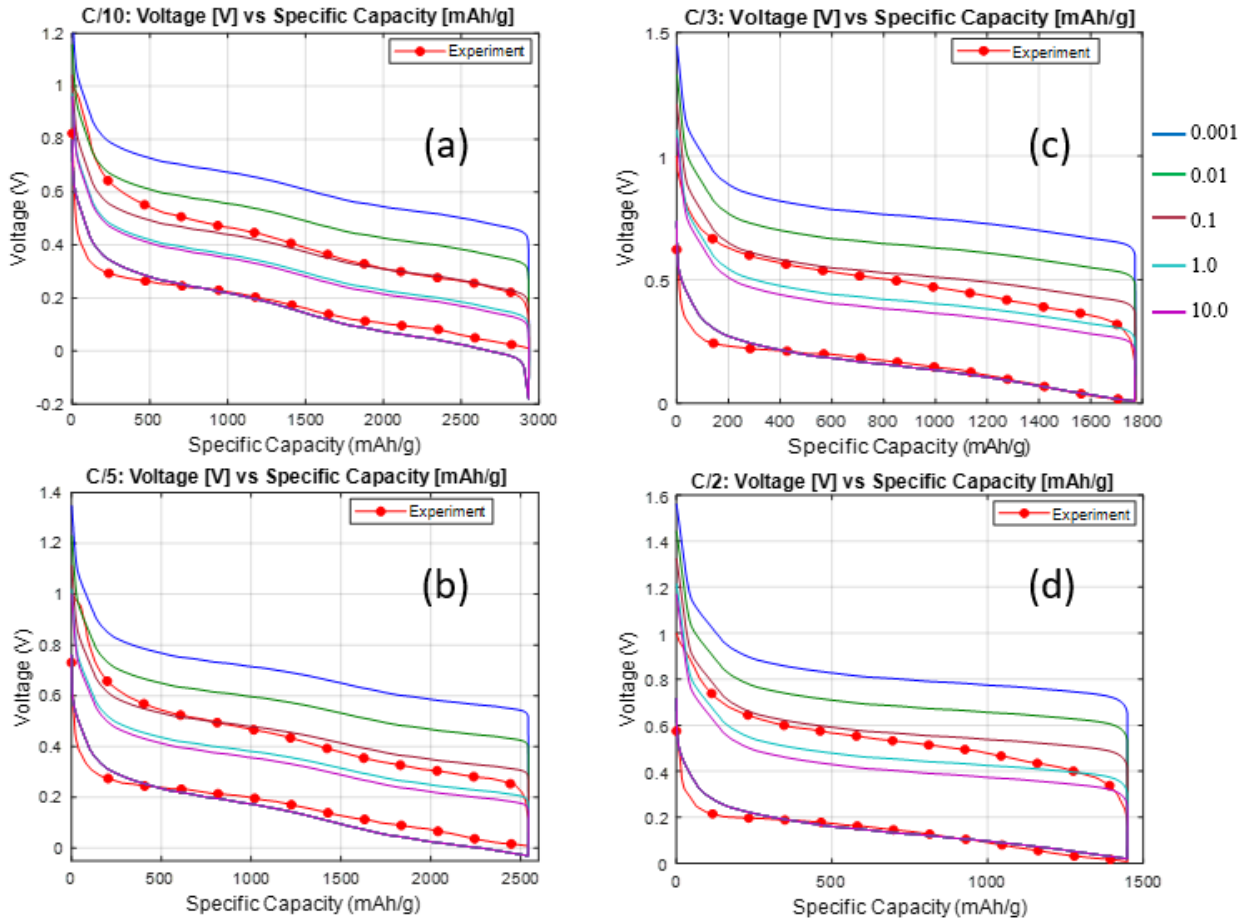

Figure-5.4: Sensitivity Analysis in Voltage vs Specific Capacity graph for different Exchange Current Density in delithiation cycle. Results of different C-Rates: C/10 (a), C/5 (b), C/3 (c), C/2 (d) have been demonstrated.

Table-5.4: Parametric ranges for sensitivity analysis of ex. current density ($i0_d$) in delithiation cycle

Exchange Current Density [A/m^2] values used in Delithiation Cycle				
0.001	0.01	0.1	1.0	10.0

In Table-5.4 the different exchange current density values which we used in simulation has been displayed. The best fitting in case of delithiation is $i0_d = 0.08$ [A/m^2].

5.1.3 Impact of Partial Molar Volume

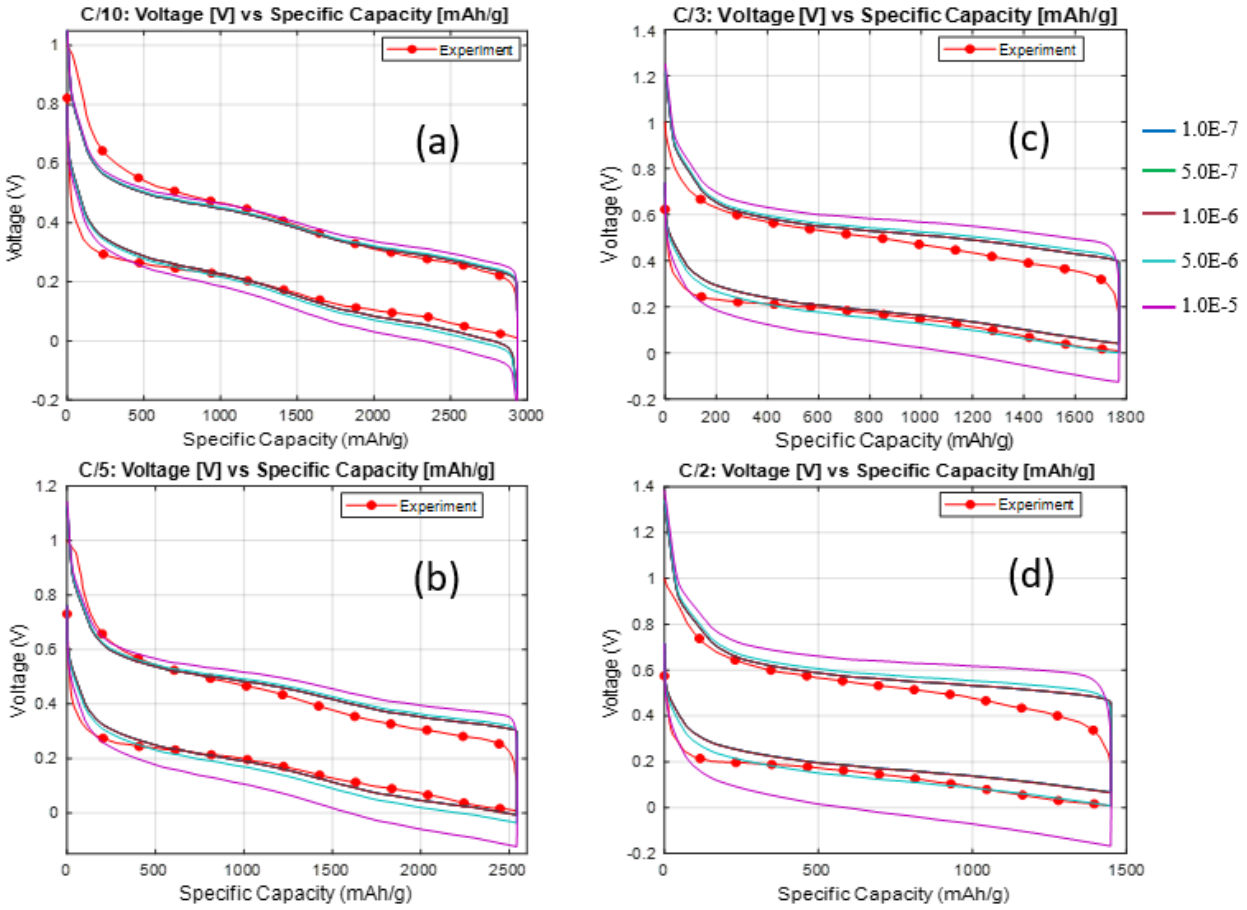

Figure-5.5: Sensitivity Analysis in Voltage vs Specific Capacity graph for different Partial Molar Volume. Results of different C-Rates: C/10 (a), C/5 (b), C/3 (c), C/2 (d) have been demonstrated.

Table-5.5: Sensitivity analysis of partial molar volume (Ω) in lithiation-delithiation cycle

Partial Molar Volume [m^3/mol] values used in Lithiation-Delithiation Cycle				
1.0E-7	5.0E-7	1.0E-6	5.0E-6	1.0E-5

At Table-5.5 the different partial molar volume values which we used in simulation has been mentioned. Here the best value we found is Ω = 4.5E-6 [m^3/mol].

5.1.4 Impact of Young's Modulus

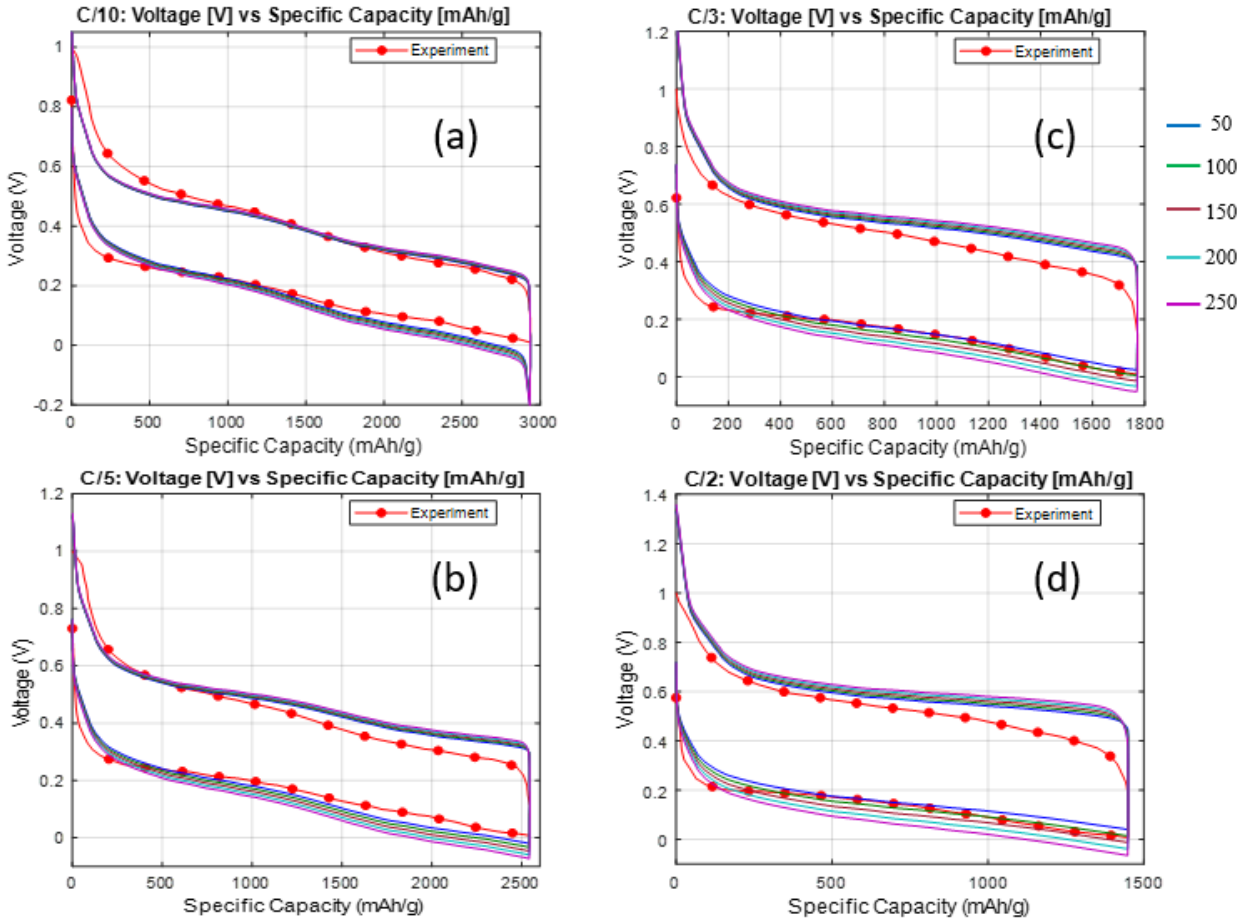

Figure-5.6: Sensitivity Analysis in Voltage vs Specific Capacity graph for different Young's Modulus. Results of different C-Rates: C/10 (a), C/5 (b), C/3 (c), C/2 (d) have been demonstrated.

Table-5.6: Sensitivity analysis of Young's modulus (E) in lithiation-delithiation cycle

Young's Modulus [GPa] values used in Lithiation-Delithiation Cycle				
50	100	150	200	250

At Table-5.5 the different Young's modulus values which we used in simulation has been highlighted. The best-fitting value we found so far is E = 90 [GPa].

5.1.5 Impact of Poisson's Ratio

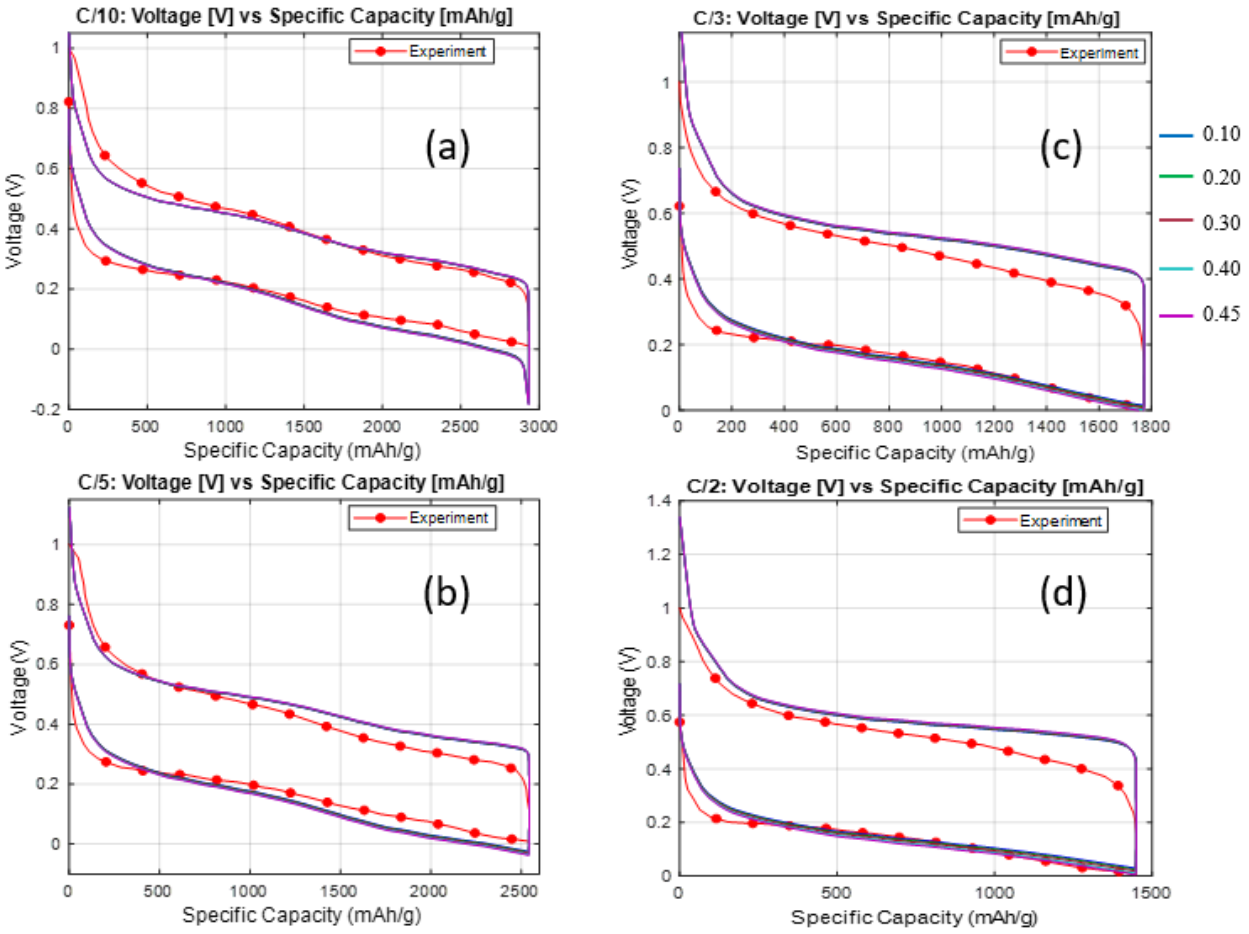

Figure-5.7: Sensitivity Analysis in Voltage vs Specific Capacity graph for different Poisson's Ratio. Results of different C-Rates: C/10 (a), C/5 (b), C/3 (c), C/2 (d) have been demonstrated.

Table-5.7: Sensitivity analysis of Poisson's ratio (ν) in lithiation-delithiation cycle

Poisson's Ratio values used in Lithiation-Delithiation Cycle				
0.10	0.20	0.30	0.40	0.45

Here, In Table-5.6, the different Poisson's ratio values that we used in simulation has been shown.

The best matched value we identified is ν=0.28.

5.2 Validation of Experimental Results

After completing the sensitivity analysis, we identified the best values for all the key parameters. The following table shows key parameters and their values,

Table-5.8: List of key parameters and their identified values used in this study

Parameters	Values	Description	Remarks
r_0	2.1 X 10^{-6}	Initial Particle Radius [m]	Ref [1]
D_l	2 X 10^{-15}	Solid Diffusivity [m^2/s] for Lithiation	Analyzed
D_d	5 X 10^{-15}	Solid Diffusivity [m^2/s] for De-lithiation	“
i_{0l}	0.006	Exchange Current Density [A/m^2] for Lithiation	“
i_{0d}	0.008	Exchange Current Density [A/m^2] for De-lithiation	“
Ω	4.5 X 10^{-6}	Partial Molar Volume [m^3/mol]	Ref [2]
E	90	Young's Modulus Constant [GPa]	“
v	0.28	Poisson's Ratio Constant	“

We validated our mathematical model using the experimental results generated by Wang et al.’s [1] battery cycling test (voltage vs specific capacity) at different C-Rates (C/10, C/5, C/3 and C/2). We also generated hydrostatic stress vs specific capacity graph and stress induced voltage vs specific capacity graph. The results are exhibited in the following section. Earlier researchers [4-6] suggested that hydrostatic stress is the main reason behind hydrostatic stress generation during battery cycling. Here, we rechecked their verdict with our own generated model. We wanted to check whether hydrostatic stress is the main reason, or any other parameters are also the factor behind this voltage gap generation.

5.2.1 Lithiation-Delithiation Cycling

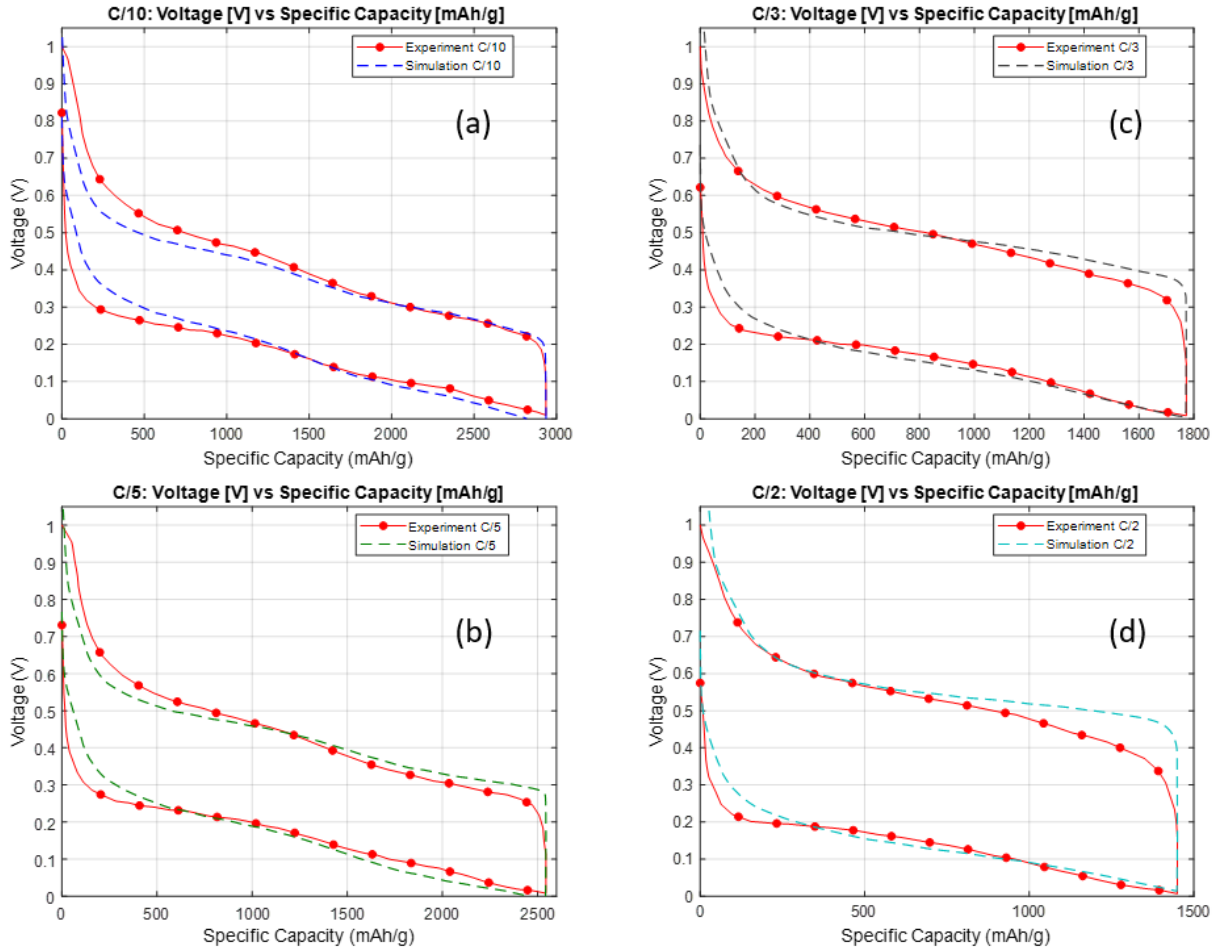

Figure-5.8: Voltage vs Specific Capacity graph for different C-Rates: C/10 (a), C/5 (b), C/3 (c), C/2 (d) have been demonstrated.

From the figure above, red dotted lines denote experimental results generated by Wang et al. [1] for four different C-Rates and dashed lines denote simulation results. For, all the C-rates we used the same parameters except Specific Capacities. For, C/10 the specific capacity was calculated 2936.00 [mAh/g], Then for C/5 it was found 2544.48 [mAh/g], Whereas for C/3 it was 1776.83 [mAh/g] and in case of C/2 specific capacity is counted as 1450.24 [mAh/g].

5.2.2 Influence of Hydrostatic Stress

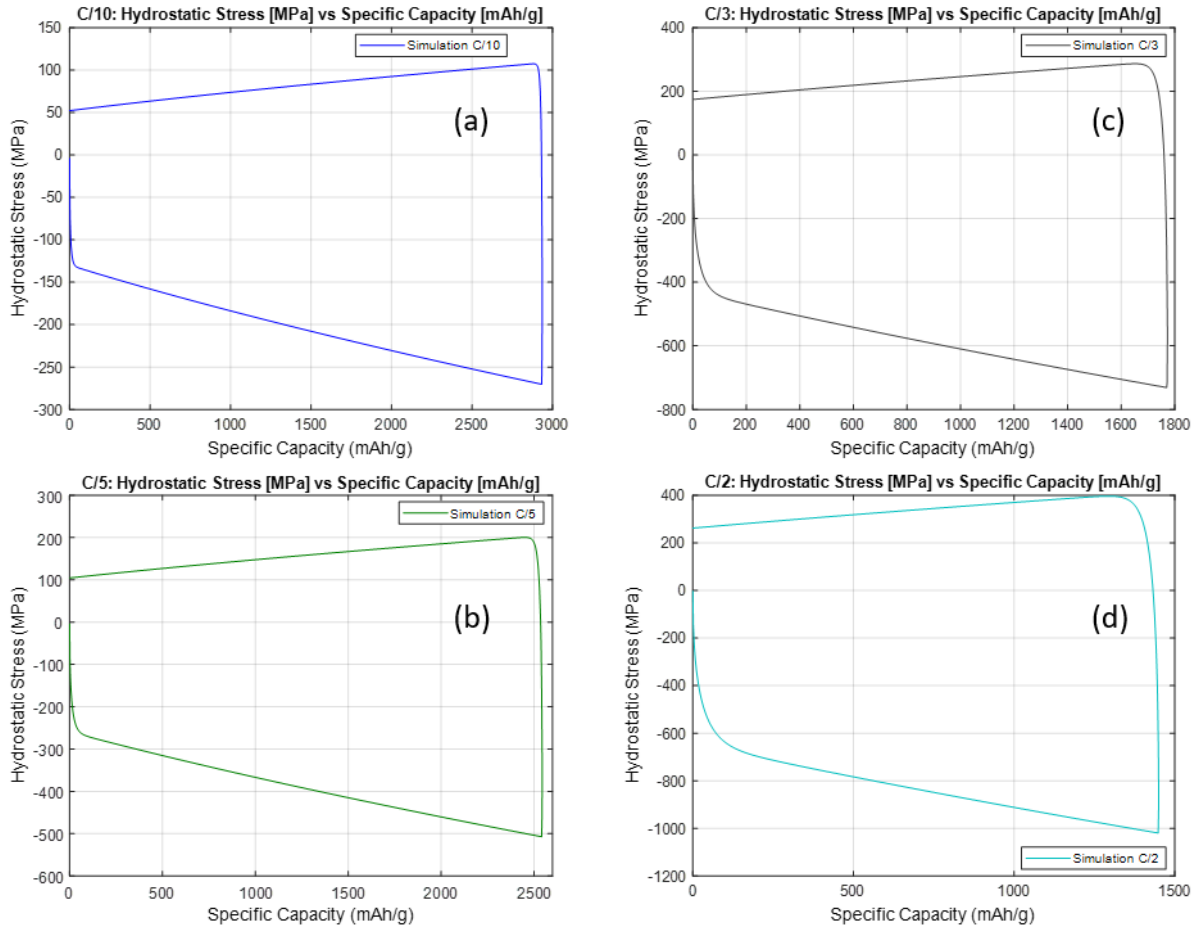

Figure-5.9: Hydrostatic Stress vs Specific Capacity graph for different C-Rates: C/10 (a), C/5 (b), C/3 (c), C/2 (d) have been demonstrated.

In the figure above hydrostatic stress vs specific capacity graphs are generated for all C-Rates. Hydrostatic stress was calculated by Cheng & Verbrugge's analytical solution [8]. For C/10 Maximum hydrostatic stress was found 110 [MPa], whereas for C/5 it is noticed as 200 [MPa], Again, In C/3 stress counted as 250 [MPa] and for C/2 we found hydrostatic stress value as 400 [MPa]. As long as C-Rates progresses hydrostatic stress keeps increasing.

5.2.3 Influence of Stress Induced Voltage

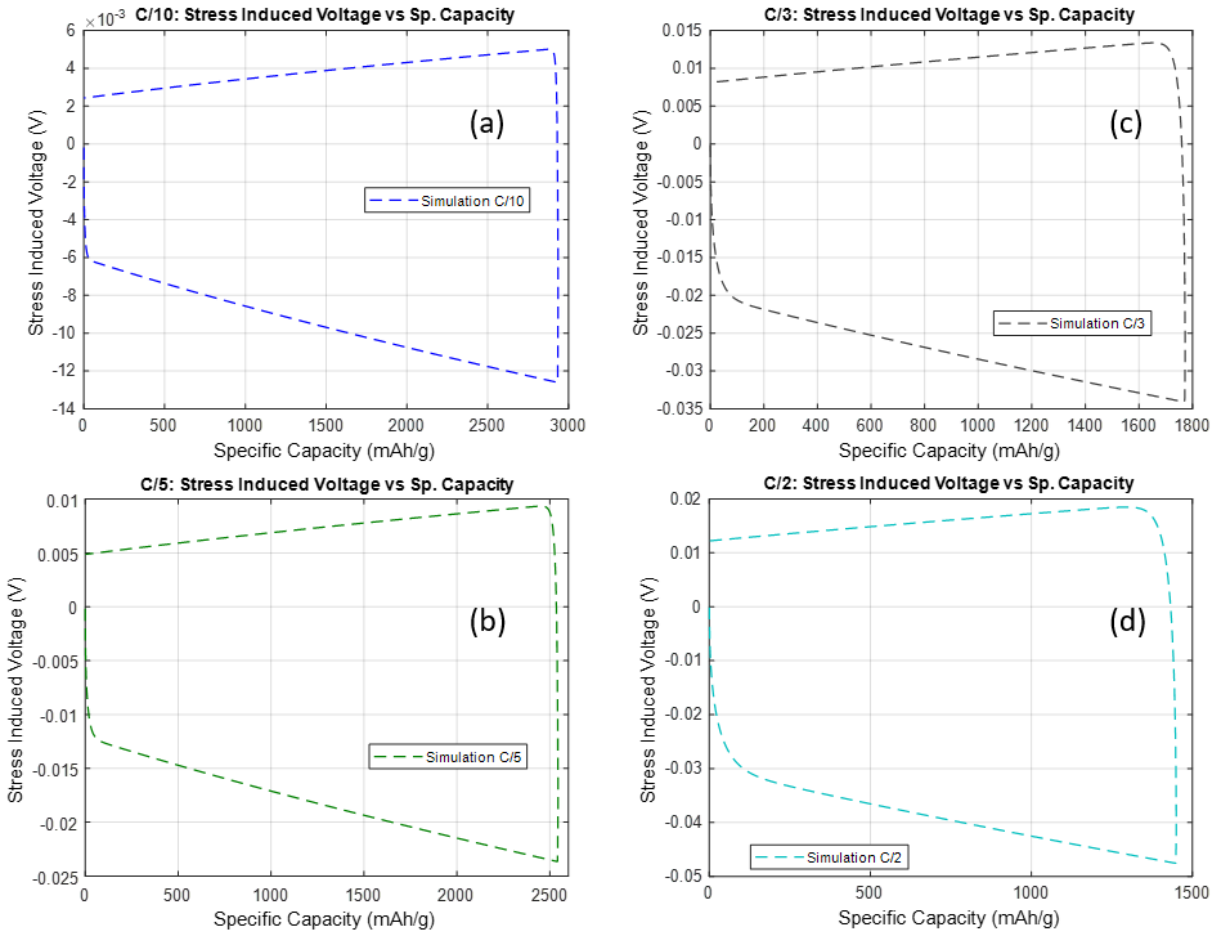

Figure-5.10: Stress Induced Voltage vs Specific Capacity graph for different C-Rates: C/10 (a), C/5 (b), C/3 (c), C/2 (d) have been demonstrated.

We also calculated stress induced voltage ($\sigma_h\Omega/F$) [V] generated from hydrostatic stress. The following table exhibits the values for four different C-Rates,

Table-5.9: Impact of stress induced voltage ($\sigma_h\Omega/F$) [V]

	C-Rates	**C/10**	**C/5**	**C/3**	**C/2**
Stress Induced Voltage, $\sigma_h\Omega/F$ [V]	Maximum	0.005	0.009	0.0014	0.018
	Minimum	-0.013	-0.024	-0.034	-0.048

From Table-5.8, it is noticed that, for all the C-Rates maximum stress induced voltage is measured as 0.018 [V] which is significantly low to have an impact on voltage hysteresis generation.

5.3 Discussion

From the results we witnessed, after including volume expansion phenomenon, asymmetric solid diffusivity, and asymmetric exchange current density in our model a good fit with experimental results of Wang et al. [1] can be found. Hydrostatic stress induced voltage is also calculated using our model. It can be noticed clearly that the maximum value of this stress induced voltage is too small ~0.018 [V] to generate voltage hysteresis during battery cycling. Using asymmetric diffusivity and asymmetric exchange current density instead helped to get a good fit with experimental results. Therefore, it can be stated that hydrostatic stress is not the sole contributor to voltage hysteresis generation. Solid diffusivity and exchange current density are equally important for the voltage hysteresis phenomenon.

5.4 References

[1] C. Wang, H. Wu, Z. Chen, M. McDowell, Y. Cui, Z. Bao, Self-healing chemistry enables the stable operation of silicon microparticle anodes for high-energy lithium-ion batteries, Nature Chemistry. 5 (2013) 1042-1048. doi:10.1038/nchem.1802.

[2] S. Pal, S.S. Damle, S.H. Patel, M.K. Datta, P.N. Kumta, S. Maiti, Modeling the delamination of amorphous-silicon thin film anode for lithium-ion battery, J. Power Sources 246 (2014) 149e159. doi.org/10.1016/j.jpowsour.2013.06.089.

[3] M. Wang, X. Xiao, X. Huang, A multiphysics microstructure-resolved model for silicon anode lithium-ion batteries, Journal of Power Sources. 348 (2017) 66-79. doi:10.1016/j.jpowsour.2017.02.037.

[4] C. Jin, H. Li, Y. Song, B. Lu, A. Soh, J. Zhang, On stress-induced voltage hysteresis in lithium ion batteries: Impacts of surface effects and inter-particle compression, Science China Technological Sciences. 62 (2019) 1357-1364. doi:10.1007/s11431-018-9491-6.

[5] Y. Song, A. Soh, J. Zhang, On stress-induced voltage hysteresis in lithium ion batteries: impacts of material property, charge rate and particle size, Journal of Materials Science. 51 (2016) 9902-9911. doi:10.1007/s10853-016-0223-y.

[6] B. Lu, Y. Song, Q. Zhang, J. Pan, Y. Cheng, J. Zhang, Voltage hysteresis of lithium ion batteries caused by mechanical stress, Physical Chemistry Chemical Physics. 18 (2016) 4721-4727. doi:10.1039/c5cp06179b.

[7] A.A. Hossain, Y. Cha, M. Song, S.U. Kim, Side Reaction Correction and Non-linear Exchange Current Density for Mathematical Modeling of Silicon Anode Based Lithium-Ion Batteries, (2020). doi:10.13140/RG.2.2.36674.40646.

[8] Y. Cheng, M. Verbrugge, The influence of surface mechanics on diffusion induced stresses within spherical nanoparticles, Journal of Applied Physics. 104 (2008) 083521. doi:10.1063/1.3000442.

[9] L. Baggetto, J.F.M. Oudenhoven, T. van Dongen, J.H. Klootwijk, M. Mulder, R.A.H. Niessen, M.H.J.M. de Croon, P.H.L. Notten, On the electrochemistry of an anode stack for all-

solid-state 3D-integrated batteries, J. Power Sources 189 (2009) 402e410. doi.org/10.1016/j.jpowsour.2008.07.076.

[10] B. Liang, Y. Liu, Y. Xu, Silicon-based materials as high capacity anodes for next generation lithium ion batteries, Journal of Power Sources. 267 (2014) 469-490. doi:10.1016/j.jpowsour.2014.05.096.

[11] L. Beaulieu, K. Eberman, R. Turner, L. Krause, J. Dahn, Colossal Reversible Volume Changes in Lithium Alloys, Electrochemical And Solid-State Letters. 4 (2001) A137. doi:10.1149/1.1388178.

CHAPTER 6: FUTURE WORK

We started our work with one-dimensional single spherical model development. We wanted to make our model as simple as possible. We added volume expansion phenomenon, state of charge (SOC) based particle radius, asymmetric solid diffusivity, asymmetric exchange current density in our model. We are the first one to do so in the battery model arena. However, in our present work, we neglected the inclusion of solid phase potential, solution phase potential and solution phase concentration. We also did not include the cathodic part in model development. In future, we have a concrete plan to include those features. Table-6.1 indicates how we will implement all the additional equations in the half-cell model. Our next plan is to convert one-dimensional model into a two-dimensional (2D) model as mentioned in Figure-6.1

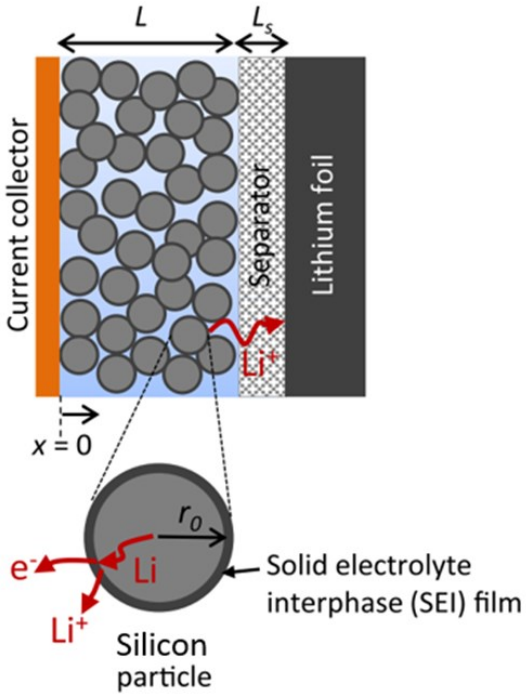

Figure-6.1: Schematic diagram of the electrode (half-cell) model developed in this study [1]

Table-6.1: Governing equations and boundary conditions used for modeling the cell

Governing Equations	Boundary conditions
Mass Conservation in Solid Phase (spherical coordinate) $\frac{\partial C_{s,i}}{\partial t} = \frac{D_s}{r^2}\frac{\partial}{\partial r}\left(r^2\frac{\partial C_{s,i}}{\partial r}\right)$	(6.1) $\left.\frac{\partial C_{s,i}}{\partial r}\right\|_{r=0} = 0, -D_s\left.\frac{\partial C_s}{\partial r}\right\|_{r=r_0} = \frac{i_i}{F}$
Mass Conservation in Electrolyte phase $\varepsilon_i\frac{\partial C_{e,i}}{\partial t} = \frac{\partial}{\partial x}\left(D_{eff,i}\frac{\partial C_{e,i}}{\partial x}\right) + (1-t_+^0)a_iJ_i$	(6.2) $-D_{eff,i}\left.\frac{\partial C_{e,i}}{\partial x}\right\|_{x=0} = -D_{eff,i}\left.\frac{\partial C_{e,i}}{\partial x}\right\|_{x=L+L_s} = 0$
Conservation of Charge in Solid Phase $\sigma_{eff,i}\frac{\partial^2\emptyset_{s,i}}{\partial x^2} = a_iFJ_i$	(6.3) $\sigma_{eff,i}\left.\frac{\partial\emptyset_{s,i}}{\partial x}\right\|_{x=0} = I_{app}, \sigma_{eff,i}\left.\frac{\partial\emptyset_{s,i}}{\partial x}\right\|_{x=L+L_s} = 0$
Conservation of Charge in Electrolyte Phase $\frac{\partial}{\partial x}\left(\kappa_{eff,i}\frac{\partial\emptyset_{e,i}}{\partial x}\right) + \frac{2RT\kappa_{eff,i}}{F}\frac{\partial}{\partial x}\left(\frac{\partial lnc_e}{\partial x}\right) = -a_iFJ_i$	(6.4) $-\kappa_{eff,i}\left.\frac{\partial\emptyset_{e,i}}{\partial x}\right\|_{x=0} = -\kappa_{eff,i}\left.\frac{\partial\emptyset_{e,i}}{\partial x}\right\|_{x=L+L_s} = 0$
Modified Butler-Volmer Kinetic Equation $V = U + \frac{\sigma_h\Omega}{\mathrm{F}} + \frac{2RT}{F}\sinh^{-1}\left(\frac{i_{app}}{2i_0a_VLF}\right) + \emptyset_s + \emptyset_e$	(6.5)
Effective properties $\kappa_{eff} = \kappa\varepsilon_e^{\gamma}$ $D_{eff} = D_e\varepsilon_e^{\gamma}$ $\sigma_{eff,i} = \varepsilon_s\sigma$	Specific interfacial surface area $a_i = \frac{3\varepsilon_s}{r_0}$ Diffusion coefficient in electrolyte phase $D_e = 10^{-4}\times 10^{-4.43-\left(\frac{54}{T-229-5.0\times10^{-3}c_i}\right)-0.22\times10^{-3}c_i}$ [2] Ionic conductivity in electrolyte phase $\kappa_{i,e} = 10^{-4}\times c_i(-10.5+0.688\times10^{-3}c_i+0.494\times10^{-6}c_i^2+0.074T-1.78\times10^{-5}c_iT-8.86\times10^{-10}c_i^2T-6.96\times10^{-5}T^2+2.80\times10^{-8}c_iT^2)^2$ [2]

The boundary conditions are the same as mentioned in the figure and the table above. Then, we will generate a model like our current SPM model. Once we are done with that, then we will modify our current mass diffusion equation with Zhang et al.'s [3] where the hydrostatic stress part is included with the equation. Next, we will repeat the same results and check the status.

$$\frac{\partial c}{\partial t} = D\frac{\partial}{\partial r}\left(\frac{\partial c}{\partial r} - \frac{\Omega c}{RT}\frac{\partial\sigma_h}{\partial r}\right) \qquad [6.6]$$

Two boundary conditions for mass diffusion equations will be implemented like below,

$$D\left(\frac{\partial c}{\partial r}-\frac{\Omega c}{RT}\frac{\partial \sigma_h}{\partial r}\right)=-\frac{i_n}{F}\;;when,\; r=R \qquad [6.7]$$

$$D\left(\frac{\partial c}{\partial r}-\frac{\Omega c}{RT}\frac{\partial \sigma_h}{\partial r}\right)=0\;;when,\; r=0 \qquad [6.8]$$

Likewise, previous equations at the center of the particle, the flux will be zero whereas at the surface of the particle flux will have impact and flux is generated using Butler-Volmer (BV) [4] equation. First, we will include this modified mass diffusion equation at our single particle model (SPM). Then, we will generate voltage vs specific capacity, hydrostatic stress vs specific capacity and voltage induced stress vs specific capacity graph. Later, we will produce same results developing full cell model.

CHAPTER 7: CONCLUSION

From our observation, it is identified, hydrostatic stress is not the sole contributor to voltage hysteresis phenomena occurring during lithiation-delithiation cycling of silicon anode-based lithium-ion batteries. In the past, Jin et al. [5], Song et. al. [6] and some other groups [7,8] gave their verdict that hydrostatic stress is the main reason behind voltage hysteresis. But none of them considered volume expansion and contraction of spherical particles, they also ignored surface crack generation phenomenon. Most important thing, they did not include any experimental data to validate their mathematical model. That left big a question for the acceptancy of their verdict. Therefore, we wanted to recheck that before developing our own mathematical model. Before developing our own model, we did some literature surveys and identified the lacking on other researchers' work. We tried to build our model very simple starting with a one-dimensional (1D) single particle model. But we made sure we include volume expansion, SOC based particle radius equation, asymmetric diffusivity & exchange current density in our model to make a realistic one. Several groups [12-15] have reported how important role volumetric change plays in silicon anode cells. Therefore, it is really important to consider this phenomenon while developing a model. Another crucial case is the emergence of surface cracks at the surface of the electrode. Researchers discussed those in their respected work [16-18]. On the other hand, Li et al. [19] reported that diffusivity cannot be same for both lithiation and delithiation cycle and same can be said for exchange current density as well. Because of these verdicts, we included these important phenomena in our model development. We collected experimental data generated by Wang et al. [1]. Then, we identified key parameters that can control the overall result of the model. Then, we conducted sensitivity analysis with those key parameters such as solid diffusivity, Exchange

current density, partial molar volume, Young's modulus and Poisson's ratio. After completing sensitivity analysis, we identified the best values for the previously mentioned parameters. Then, we generated voltage vs specific capacity, hydrostatic stress vs specific capacity and stress induced voltage vs specific capacity graphs for four different C-Rates (C/10, C/5, C/3 & C/2). We validated the model with experimental results. We noticed that, for all C-Rates maximum hydrostatic stress induced voltage is 0.0018 [V] which is significantly low to have an impact on voltage hysteresis generation. On the other hand, the inclusion of SOC dependent particle radius equation, asymmetric solid diffusivity and asymmetric exchange current density assisted our model to make a good fit with experimental results. Therefore, it can be stated, not only hydrostatic stress but also solid diffusivity and exchange current density are equally important for voltage hysteresis emergence during battery cycling in silicon anode-based lithium half cells.

REFERENCES

[1] K. Takahashi, V. Srinivasan, Examination of Graphite Particle Cracking as a Failure Mode in Lithium-Ion Batteries: A Model-Experimental Study, Journal of The Electrochemical Society. 162 (2015) A635-A645. doi:10.1149/2.0281504jes.

[2] L. Valøen, J. Reimers, Transport Properties of LiPF[sub 6]-Based Li-Ion Battery Electrolytes, Journal Of The Electrochemical Society. 152 (2005) A882. doi:10.1149/1.1872737.

[3] X. Zhang, W. Shyy, A. Marie Sastry, Numerical Simulation of Intercalation-Induced Stress in Li-Ion Battery Electrode Particles, Journal of The Electrochemical Society. 154 (2007) A910. doi:10.1149/1.2759840.

[4] A.A. Hossain, Y. Cha, M. Song, S.U. Kim, Side Reaction Correction and Non-linear Exchange Current Density for Mathematical Modeling of Silicon Anode Based Lithium-Ion Batteries, (2020). doi:10.13140/RG.2.2.36674.40646.

[5] C. Jin, H. Li, Y. Song, B. Lu, A. Soh, J. Zhang, On stress-induced voltage hysteresis in lithium ion batteries: Impacts of surface effects and inter-particle compression, Science China Technological Sciences. 62 (2019) 1357-1364. doi:10.1007/s11431-018-9491-6.

[6] Y. Song, A. Soh, J. Zhang, On stress-induced voltage hysteresis in lithium ion batteries: impacts of material property, charge rate and particle size, Journal of Materials Science. 51 (2016) 9902-9911. doi:10.1007/s10853-016-0223-y.

[7] B. Lu, Y. Song, Q. Zhang, J. Pan, Y. Cheng, J. Zhang, Voltage hysteresis of lithium ion batteries caused by mechanical stress, Physical Chemistry Chemical Physics. 18 (2016) 4721-4727. doi:10.1039/c5cp06179b.

[8] S. Pal, S.S. Damle, S.H. Patel, M.K. Datta, P.N. Kumta, S. Maiti, Modeling the delamination of amorphous-silicon thin film anode for lithium-ion battery, J. Power Sources 246 (2014) 149e159. doi.org/10.1016/j.jpowsour.2013.06.089

[9] R. Deshpande, Y. Cheng, M. Verbrugge, Modeling diffusion-induced stress in nanowire electrode structures, Journal of Power Sources. 195 (2010) 5081-5088. doi:10.1016/j.jpowsour.2010.02.021.

[10] A. Bower, P. Guduru, V. Sethuraman, A finite strain model of stress, diffusion, plastic flow, and electrochemical reactions in a lithium-ion half-cell, Journal of The Mechanics and Physics of Solids. 59 (2011) 804-828. doi:10.1016/j.jmps.2011.01.003.

[11] M. Wang, X. Xiao, X. Huang, A multiphysics microstructure-resolved model for silicon anode lithium-ion batteries, Journal of Power Sources. 348 (2017) 66-79. doi:10.1016/j.jpowsour.2017.02.037.

[12] H. Wu, Y. Cui, Designing nanostructured Si anodes for high energy lithium ion batteries, Nano Today. 7 (2012) 414-429. doi:10.1016/j.nantod.2012.08.004.

[13] M. Ashuri, Q. He, L. Shaw, Silicon as a potential anode material for Li-ion batteries: where size, geometry and structure matter, Nanoscale. 8 (2016) 74-103. doi:10.1039/c5nr05116a.

[14] M. Verbrugge, D. Baker, X. Xiao, Q. Zhang, Y. Cheng, Experimental and Theoretical Characterization of Electrode Materials that Undergo Large Volume Changes and Application to the Lithium–Silicon System, The Journal of Physical Chemistry C. 119 (2015) 5341-5349. doi:10.1021/jp512585z.

[15] Q. Wu, B. Shi, J. Bareño, Y. Liu, V. Maroni, D. Zhai et al., Investigations of Si Thin Films as Anode of Lithium-Ion Batteries, ACS Applied Materials & Interfaces. 10 (2018) 3487-3494. doi:10.1021/acsami.7b13980.

[16] Y. Jin, B. Zhu, Z. Lu, N. Liu, J. Zhu, Challenges and Recent Progress in the Development of Si Anodes for Lithium-Ion Battery, Advanced Energy Materials. 7 (2017) 1700715. doi:10.1002/aenm.201700715.

[17] A. Basak, J. Fan, J. Wang, P. Mathew, Material removal mechanisms of monocrystalline silicon under the impact of high velocity micro-particles, Wear. 269 (2010) 269-277. doi:10.1016/j.wear.2010.04.006.

[18] M. Gu, Y. He, J. Zheng, C. Wang, Nanoscale silicon as anode for Li-ion batteries: The fundamentals, promises, and challenges, Nano Energy. 17 (2015) 366-383. doi:10.1016/j.nanoen.2015.08.025.

[19] J. Li, N. Dudney, X. Xiao, Y. Cheng, C. Liang, M. Verbrugge, Asymmetric Rate Behavior of Si Anodes for Lithium-Ion Batteries: Ultrafast De-Lithiation versus Sluggish Lithiation at High Current Densities, Advanced Energy Materials. 5 (2014) 1401627. doi:10.1002/aenm.201401627.

[20] J. Christensen, Modeling Diffusion-Induced Stress in Li-Ion Cells with Porous Electrodes, Journal of The Electrochemical Society. 157 (2010) A366. doi:10.1149/1.3269995.